Solid Earth, 13, 1259–1280, 2022
https://doi.org/10.5194/se-13-1259-2022

Solid Earth Open Access EGU

Whole-rock and zircon evidence for evolution of the Late Jurassic high-Sr / Y Zhoujiapuzi granite, Liaodong Peninsula, North China Craton

Renyu Zeng[1,2,3], Mark B. Allen[3], Xiancheng Mao[4], Jianqing Lai[4], Jie Yan[1,2], and Jianjun Wan[1,2]

[1]State Key Laboratory of Nuclear Resources and Environment, East China University of Technology, Nanchang, 330013, Jiangxi, China
[2]School of Earth Sciences, East China University of Technology, Nanchang, 330013, China
[3]Department of Earth Sciences, Durham University, Durham, DH1 3LE, UK
[4]School of Geosciences and Info-Physics, Central South University, Changsha, 410083, China

Correspondence: Renyu Zeng (zengrenyu@126.com)

Received: 15 October 2021 – Discussion started: 17 November 2021
Revised: 24 June 2022 – Accepted: 28 July 2022 – Published: 12 August 2022

Abstract. Middle–Late Jurassic high-Sr/Y granitic intrusions are extensively exposed in the Liaodong Peninsula in the eastern part of the North China Craton (NCC). However, the genesis of the high Sr/Y signature in these intrusions has not been studied in detail. In this study, we report results of zircon U–Pb dating, Hf isotopic analysis, and zircon and whole-rock geochemical data for the Late Jurassic Zhoujiapuzi granite in the middle part of the Liaodong Peninsula. The Zhoujiapuzi granite is high-K (calc–alkaline) and peraluminous in nature, with high SiO_2 (68.1 wt %–73.0 wt %) and Al_2O_3 (14.5 wt %–16.8 wt %), low TFe_2O_3 (1.10 wt %–2.49 wt %) and MgO (0.10 wt %–0.44 wt %), and high Sr/Y (19.9–102.0) and La_N/Yb_N (14.59–80.40), which is characteristic of high-Sr/Y I-type granite. The geochemical signatures, in combination with the presence of a large number of Paleoproterozoic inherited zircons, indicate that the Zhoujiapuzi granite was most likely derived from partial melting of the basement in the region, specifically the Liaoji granites. The high Sr/Y signature is inherited from these source rocks. Laser ablation–inductively coupled plasma mass spectrometer (LA-ICP-MS) zircon U–Pb dating of the autocryst zircons from two samples (from different localities) yielded consistent weighted average ages of 160.7 ± 1.1 Ma (mean squared weighted deviation – MSWD = 1.3) and 159.6 ± 1.1 Ma (MSWD = 1.2), with $\varepsilon Hf(t)$ values in the range of −26.6 to −22.8. Morphological and chemical studies on autocrystic zircon grains show that there are two stages of zircon growth, interpreted as magmatic evolution in two distinct stages. The light-cathodoluminescence (light-CL) core reflects a crystallization environment of low oxygen fugacity and high T_{Zr-Ti}; the dark-CL rim formed with high oxygen fugacity and lower T_{Zr-Ti}. Based on the geochemical features and regional geological data, we propose that the Liaodong Peninsula in the Late Jurassic was part of a mature continental arc, with extensive melting of thick crust above the Paleo-Pacific subduction zone.

1 Introduction

The Liaodong Peninsula is located in the northeast of the North China Craton (NCC). The northeastern NCC was influenced by three main tectonic regimes in the Mesozoic related to the subduction of the Paleo-Asian, Paleo-Pacific, and Mongol–Okhotsk oceans (Tang et al., 2018). The superposition of these different regimes resulted in changing tectonic and magmatic patterns over time. Middle–Late Jurassic granitic rocks are extensively exposed in the northern parts of the Liaodong Peninsula, such as the Yutun mylonitic granite, Xiaoheishan granodiorite, Heigou monzogranite (Wu et al., 2005a), Wulong two-mica monzogranite (Yang et al., 2018), and Huangdi biotite monzogranite (Xue et al., 2020). Most of these rocks are characterized by high Sr/Y and plot within

the adakite field on Sr/Y–Y and La_N/YbN–Yb_N diagrams (Wu et al., 2005a; F. C. Yang et al., 2015, 2018).

The geodynamic settings and petrogenesis of adakite and geochemically similar high-Sr/Y igneous rocks have been widely discussed. The high-Sr/Y rocks were originally proposed to have been formed by melting of young (< 25 Ma) and hot subducted oceanic slab in an arc setting (Defant and Drummond, 1990). However, later studies have shown that the high-Sr/Y rocks can form in both arc and non-arc settings by other processes, such as continental interior settings (Wang et al., 2007), cold subduction zones (Nakamura and Iwamori, 2013), and collision or post-collision processes (Schwartz et al., 2011). In addition, numerous studies have suggested that the lower continental crust can also be the source of the high-Sr/Y rocks (Gao et al., 2004; Ou et al., 2017). However, it is debated whether crustal thickening is necessary for their formation (e.g., Moyen, 2009; Kamei et al., 2009; Zhan et al., 2020). In recent years, some studies have proposed that the high Sr/Y ratio in granitic rocks can be inherited from a high-Sr/Y crust source, regardless of pressure (Kamei et al., 2009; Ma et al., 2015; Zhan et al., 2020).

The Middle–Late Jurassic granitic rocks in the Liaodong Peninsula are commonly proposed to be the products of partial melting of thickened mafic crust with garnet in the residue (Wu et al., 2005a; F. C. Yang et al., 2015, 2018; Tang et al., 2018). However, the source composition has not been fully considered in the petrogenesis of the high-Sr/Y rocks in the Liaodong Peninsula. Hence, the petrogenesis of the Middle–Late Jurassic high-Sr/Y rocks needs to be re-evaluated based on more detailed work and a consideration of possible sources. This petrogenesis is of significance for understanding the Jurassic tectonics of the Liaodong Peninsula and the NCC in general.

In this paper, we examined the high-Sr/Y Zhoujiapuzi granite from the Xiuyan area in the middle of the Liaodong Peninsula. Zircons are analyzed for U–Pb–Hf isotopes and trace element geochemistry, as well as by Raman spectroscopy. These results are integrated with whole-rock geochemistry. We focus on the zircons because of their potential to reveal the origins of the pluton (Belousova et al., 2002; Wang et al., 2007; Breiter et al., 2014; Zhao et al., 2014) and provide a case study for the evolution of plutonic magma systems in general. Based on observations of the CL images and chemical analysis, two zircon growth stages can be distinguished. We first determine the crystallization environments of the two zircon growth stages and then decipher the petrogenesis, source characteristics, and origin of the high Sr/Y signature of the pluton as a whole. Integrated with previous studies, our study provides insights into the tectonic evolution of the Liaodong Peninsula in the Late Jurassic.

2 Geological setting

The Zhoujiapuzi granite is located in the middle of the Liaodong Peninsula at the northeastern margin of the NCC (Fig. 1). The Paleoproterozoic Liaohe Group and Liaoji granite are the basement in the study area. The Liaohe Group includes the Lieryu, Gaojiayu, Dashiqiao, and Gaixian formations. Although stratigraphic terms are used, these rocks are metamorphic, and the group consists of leptynite, leptite, granulite, amphibolite, marble, and phyllite. The protoliths of the Liaohe Group include marine volcanics, clastics, carbonates, and claystones. The formation age of the metasedimentary rocks in the Liaohe Group is 2.0–1.9 Ga (Wan et al., 2006; Li et al., 2015). It is in unconformable contact with the overlying strata of the Mesoproterozoic Cuocaogou Formation and Xiaoling Formation.

The study area experienced strong magmatic activity in the Paleoproterozoic, which can be divided into two stages of 2.2–2.1 and ∼ 1.85 Ga. The 2.18–2.14 Ga Liaoji granites (also called gneissic granites), which lie within an area measuring 300 km × 70 km, are dominated by A- and I-type granites (Li and Zhao, 2007; Yang et al., 2016; X. P. Wang et al., 2020). Metamorphosed volcanic rocks (leptynite, leptite, and granulite) in the Liaohe Group also formed at 2.2–2.1 Ga (Li et al., 2015). The ∼ 1.85 Ga granites mainly consist of I- and S-type porphyry granites and alkaline syenites (Yang et al., 2007; M. C. Yang et al., 2015). In addition, there were small amounts of mafic magmatic activity at ∼ 2.17, ∼ 2.1, and ∼ 1.8 Ga (Meng et al., 2014; Yuan et al., 2015). There are a variety of viewpoints on the Paleoproterozoic tectonomagmatic evolution in the Liaodong Peninsula, such as an intracontinental rift opening–closing model (Li et al., 2005) and an arc–continent collision model (Faure et al., 2004).

In the Mesozoic, the region of the Liaodong Peninsula was influenced by the circum-Pacific tectonic regime, the Mongol–Okhotsk tectonic regime, and the Paleo-Asian Ocean tectonic regime. The joint influence of multiple tectonic regimes resulted in intensive magmatism during the Mesozoic (Fig. 1b). These Mesozoic magmatic rocks can be divided into three stages, namely the Triassic (233–212 Ma), Jurassic (180–156 Ma), and Early Cretaceous (131–117 Ma) (Wu et al., 2005b).

The Triassic magmatic rocks are less exposed and are mainly alkaline rocks, diabase, diorites, and granites (Wu et al., 2005b). Among them, the granites mainly have A-type affinity and may have formed in an extensional setting (Tang et al., 2018; Wang et al., 2019). Magmatism has been related to either the subduction of the Paleo-Pacific slab, closure of the Paleo-Asian Ocean, or the collision between the NCC and the Yangtze Craton (Tang et al., 2018; Wang et al., 2019). The majority of the Jurassic magmatic rocks are monzogranite and granodiorite, which are generally calc–alkaline I-type granites, and show characteristics of adakite-like rocks. Some of them, exposed near later extensional structures, have undergone regional ductile defor-

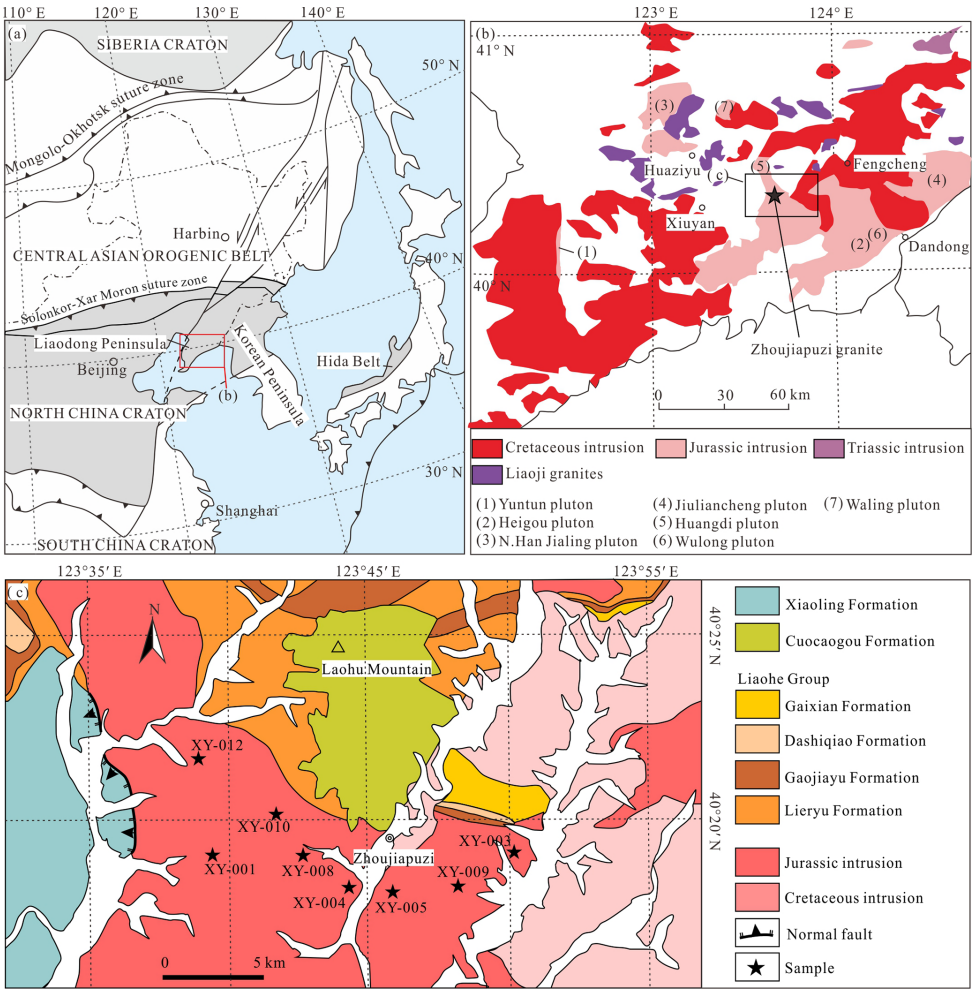

Figure 1. (a) Simplified geological map of northeastern China (modified from Li et al., 2016); **(b)** distribution of Mesozoic intrusions in the Liaodong Peninsula (modified from Wu et al., 2005a); **(c)** geological map of the Zhoujiapuzi granite.

mation. These Jurassic magmatic rocks are generally considered to relate to the subduction of the Paleo-Pacific slab (Wu et al., 2005a; Zhai et al., 2004). In the Early Cretaceous, basic–acidic–alkaline rocks were widely developed. Among them, the granites have mainly A- and I-type affinities. These rocks are generally considered to have formed in an intense extensional environment, which is connected with either the rollback or low-angle subduction of the Paleo-Pacific slab (Wu et al., 2005c; Zheng et al., 2018).

3 Samples and petrography

The Zhoujiapuzi granite is located to the east of Xiuyan in the middle of the Liaodong Peninsula (Fig. 1b). It intruded into the Lieryu Formation of the Liaohe Group. Eight samples of the Zhoujiapuzi granite were collected at locations shown in Fig. 1c.

The Zhoujiapuzi granite is generally gray in color and with fine-grained texture (Fig. 2a). The mineral assemblage contains K-feldspar (∼ 50 %), quartz (∼ 25 %), plagioclase (∼ 20 %), and biotite (∼ 5 %) as well as accessory minerals such as zircon, ilmenite, magnetite, and apatite. K-feldspar grains are euhedral or subhedral and always exhibit cross-hatched twinning (Fig. 2b). Quartz grains are usually xenomorphic and have indented boundaries and wavy extinction (Fig. 2b–d). Plagioclase always exhibits polysynthetic twinning and has sericitization in places (Fig. 2c). Biotite mainly fills in the interstices between the other minerals (Fig. 2c, d).

4 Analytical methods

The cathodoluminescence (CL) images of zircon were obtained by the Chengpu Geological Testing Co. Ltd, Langfang, China, using the Tescan Integrated Mineral Analyzer (TIMA). The LA-ICP-MS zircon U–Pb analyses were per-

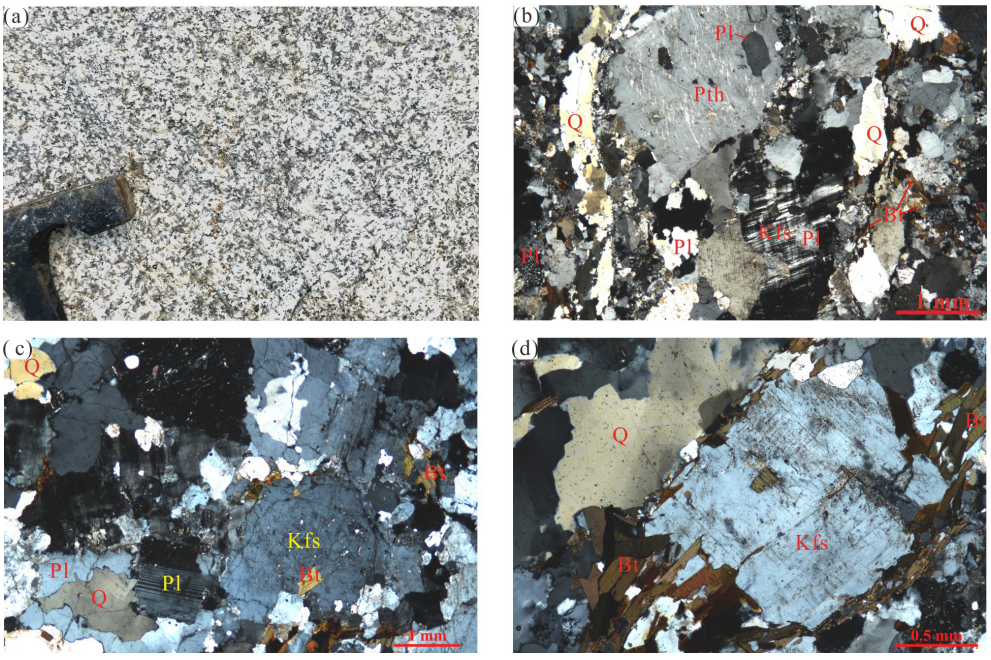

Figure 2. Outcrop photograph **(a)** and corresponding micrographs (**b, c, d** – perpendicular polarized light). Q – quartz; Kfs – feldspar; Pl – plagioclase; Pth – perthite; Bt – biotite.

formed using an Agilent Technologies 7700x ICP-MS with a Teledyne Cetac Technologies Analyte Excite laser-ablation system at Nanjing FocuMS Contract Testing Co. Ltd. The analyses were carried out with a 35 µm spot size at 8 Hz repetition rate for 40 s. The ICP-MS detector has dual modes: pulse for lower signal and analog for higher signal. Pulse–analog cross-calibration was performed before the measurement of U–Pb isotopes, delivering a wider linear dynamic range up to 10 orders of magnitude. For a signal of ^{238}U higher than 1.2×10^6–1.4×10^6 cps, equivalent zircon contains U concentrations higher than 600 ppm measured in analog mode. 91500 was used as an external standard. GJ-1 (600 Ma, Jackson et al., 2004) and Plešovice (337 Ma, Sláma et al., 2008) were treated as a quality control for geochronology. During our analyses, the weighted mean ages of GJ-1 and Plešovice were 606.0 ± 4.8 Ma ($n = 16$, MSWD = 0.50) and 340.9 ± 4.0 Ma ($n = 7$, MSWD = 1.0), respectively. Trace element abundances of zircon were externally calibrated against NIST SRM 610 with Si as the internal standard. The raw ICP-MS data were processed using ICPMSDataCal software (Liu et al., 2010). No common Pb correction was applied to the data. Data reduction was completed using the Isoplot4.15 (Ludwig, 2003). The instrument description and analytical procedure are described in detail by Zeng et al. (2018).

The in situ Lu–Hf isotopic analyses of zircon were performed by LA-MC-ICP-MS using a Teledyne Cetac laser-ablation system and a Nu Plasma II MC-ICP-MS at Nanjing FocuMS Contract Testing Co. Ltd. The 193 nm ArF excimer laser was focused on the zircon surface with a fluence of 6.0 J cm^{-2}. The ablation protocol employed a spot diameter of 50 µm at 8 Hz repetition rate for 40 s. Three standard zircons, GJ-1, 91500, and Penglai, were analyzed for quality control every 10 unknown samples. In the experiment, standard zircon GJ-1, 91500, and Penglai were analyzed, and the ^{176}Hf/^{177}Hf ratios were 0.282002–0.282013, 0.282305–0.282315, and 0.282901–0.282914, respectively, in accordance with their recommended values (GJ-1: 0.282012, Yuan et al., 2008; 91500: 0.282307 ± 0.000031, Wu et al., 2006; Penglai: 0.282906 ± 0.000010, Li et al., 2010). For the calculation of εHf(t) values, we have adopted the ^{176}Lu decay constant of 1.867×10^{-11} (Söderlund et al., 2004) and the present-day chondritic values of ^{176}Lu/^{177}Hf = 0.0332 and ^{176}Hf/^{177}Hf = 0.282772 (Blichert-Toft and Albarède 1997). To calculate one-stage model ages (T_{DM1}) relative to a depleted-mantle source, we have adopted the present-day depleted-mantle values of ^{176}Lu/^{177}Hf = 0.0384 and ^{176}Hf/^{177}Hf = 0.28325 (Vervoort and Blichert-Toft, 1999). To calculate two-stage model ages (TDM2), "felsic crust" model ages are calculated using average continental crust: ^{176}Lu/^{177}Hf = 0.015 (Griffin et al., 2004).

Zircon Raman analyses were carried out using an RM2000 laser Raman spectrometer at the State Key Laboratory of Nuclear Resources and Environment, East China University of Technology. The selected incident wavelengths were 532 and 785 nm in order to clearly identify the luminescence bands due to low concentration impurities. The beam power was 20 mW. The Leica 50× objective was employed.

Six fresh rock samples were selected for geochemical analysis. The elemental analyses were conducted at Analytical Chemistry & Testing Services (ALS) Chemex (Guangzhou) Ltd. Major oxides were analyzed using wave-dispersive X-ray fluorescence (XRF) (ME-XRF26). Analytical precision was better than ±0.01 %. Trace element abundances were measured by the lithium borate dissolution method and ICP-MS (ME-MS81). The analytical uncertainties of rare earth elements (REEs) and high-field-strength elements (HFSEs) are < 5 %. Analytical uncertainties are in the range of 5 %–10 % for the other elements. The detailed analytical procedures refer to Zhang et al. (2019) and Nash et al. (2020).

5 Analytical results

The data for major and trace elements, Raman microprobe data, zircon trace elements, zircon U–Pb ages, and zircon Hf isotopes are shown in Tables S1, S2, S3, S4, and S5 in the Supplement, respectively.

5.1 Whole-rock major and trace element compositions

SiO_2 contents range from 68.11 wt % to 73.02 wt % (average 71.71 wt %). Contents of Na_2O and K_2O are 3.81 wt %–4.65 wt % and 4.32 wt %–4.71 wt %, respectively, with an Na_2O/K_2O ratio of 0.82–1.08 and total alkalis ($Na_2O + K_2O$) of 8.38–8.97. All samples plot in the field of granite in the total alkali–silica (TAS) classification except one (Fig. 3a). These samples have Al_2O_3 contents of 14.49 wt %–16.83 wt % (average 15.09 wt %), CaO contents of 1.04 wt %–1.98 wt % (average 1.38 wt %), and A/CNK values of 1.05–1.10 (average 1.07). In the A/NK–A/CNK diagram (Fig. 3b), all samples plot in the peraluminous field (Fig. 3b). The granite samples have low TFe_2O_3 (TFe_2O_3 = all Fe calculated as Fe_2O_3) contents and MgO contents ranging from 1.10 wt %–2.49 wt % and 0.10 wt %–0.44 wt %, respectively, with Mg# (Mg# = 100 · molar Mg / (Mg + Fe)) values of 15–26.

The samples of the Zhoujiapuzi granite exhibit variable REEs, with total REEs ranging from 59 to 302 ppm. The La_N/Yb_N values of the Zhoujiapuzi granite range from 14.59 to 80.40 (average 38.27), showing right-declined REE patterns (Fig. 4a). The samples have Eu/Eu* of 0.62–1.94 and Ce/Ce* of 0.94–1.16. In the primitive mantle-normalized trace element diagram (Fig. 4b), the samples show negative anomalies of HFSEs (e.g., Nb, Ta, Ti, and P) and positive anomalies of La and large ion lithophile elements (LILEs, e.g., K, Rb, Ba, U, La, Ce). The Zhoujiapuzi granite is characterized by high contents of Sr (309–551 ppm) and low contents of Y (5.01–15.5 ppm) and Yb (0.43–1.40 ppm), with high Sr/Y ratios of 19.94–102.04 (average 65.50).

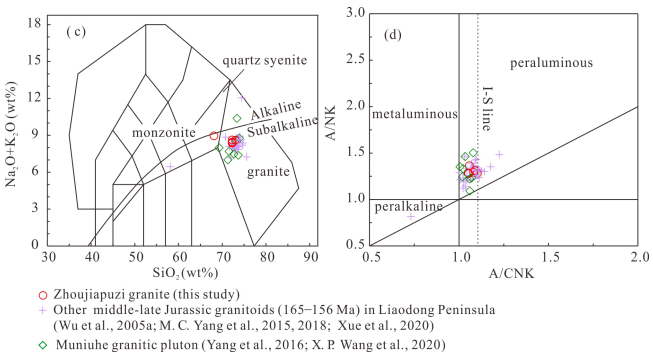

Figure 3. Geochemical classification diagrams for the Zhoujiapuzi granite. **(a)** TAS diagram (after Middlemost, 1994); **(b)** A/CNK−A/NK diagram (after Maniar and Piccoli, 1989).

5.2 Zircon CL images, Raman spectra, and REEs

CL images of zircons from the Zhoujiapuzi granite are shown in Fig. 5. Zircons commonly have crystal sizes between 150 and 250 µm and have length-to-width ratios of 2 : 1–4 : 1, with euhedral, stubby to elongate prisms. According to the CL images, most zircons show an internal division into two distinct domains: a light-CL core and dark-CL rim. The light-CL core is characterized by bright CL intensity and widely spaced oscillatory zoning patterns. The dark-CL rim is overgrown continuously by the light-CL core and is characterized by extremely low CL emission and narrowly spaced oscillatory zoning patterns. In addition, some zircons have inherited cores, which have corroded and rounded shapes in contact with the light-CL core, such as 1# and 37# in XY-001 and 6# and 41# in XY-008 (Fig. 5). These inherited zircons have oscillatory zoning in CL images.

Six light-CL core spots and six dark-CL rim spots were analyzed for Raman spectra. The light-CL cores have anti-symmetric stretching vibration (B_{1g}) of the SiO_4 tetrahedra (υ_3 (SiO_4)) Raman band of 1005–1007 cm^{-1} and half-width of the υ_3 (SiO_4) Raman band (b) values of 6.0–8.1 cm^{-1}, while the dark-CL rims have υ_3 (SiO_4) Raman band of 1004–1007 cm^{-1} and b values of 5.4–9.0 cm^{-1}.

A total of 20 light-CL core spots, 18 dark-CL rim spots, and 6 inherited zircon spots were analyzed for trace and rare earth elements. The light-CL core spots have lower U content (28–677 ppm) than the dark-CL rim spots (U = 641–3842 ppm). In the chondrite-normalized REE diagram (Fig. 6a, b), both the light-CL core and dark-CL rim are characterized by HREE enrichment relative to LREE with positive Ce anomalies and negative Eu anomalies. The light-CL core spots have ΣREE of 49–1115 ppm (average 390 ppm), ΣLREE of 3–72 ppm (average 14 ppm), and ΣHREE of 46–1100 ppm (average 377 ppm), whereas the dark-CL rim spots have ΣREE of 327–1632 ppm (average 895 ppm), ΣLREE of 2–14 ppm (average 6 ppm), and ΣHREE of 325–1627 ppm (average 889 ppm). Hence, the

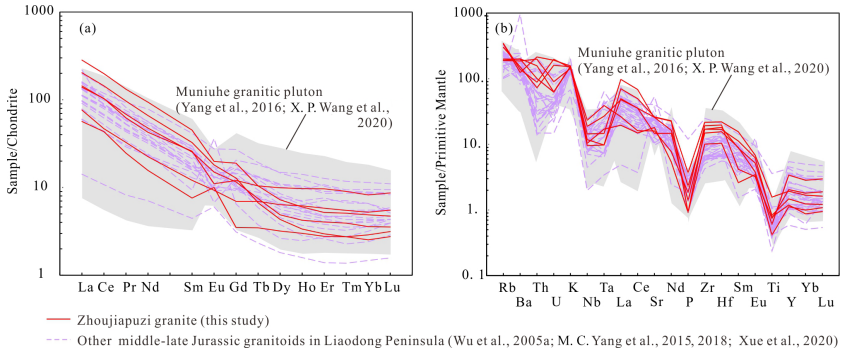

Figure 4. Chondrite-normalized REE patterns and primitive mantle-normalized trace element patterns of the Zhoujiapuzi granite (chondrite and primitive mantle values are from Sun and McDonough, 1989).

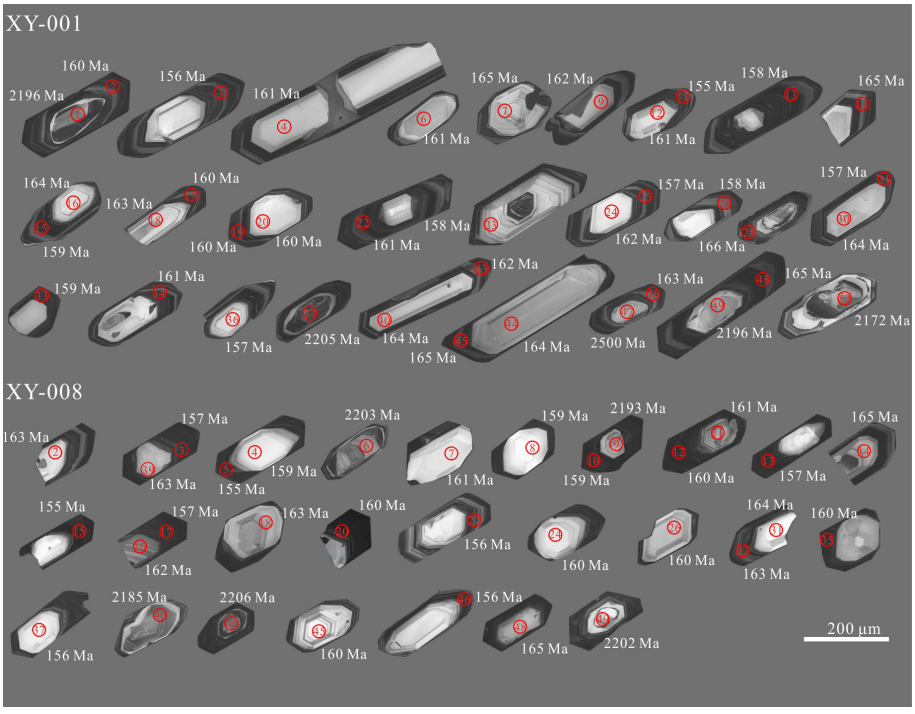

Figure 5. CL images of zircons. Circles denote U–Pb analysis spot. Numbers in the circles are the spot numbers. Numbers near the analytical spots are the U–Pb ages (Ma).

REE content of the light-CL core is significantly lower than that of the dark-CL rim, and the difference between the two is mainly in HREE content. The light-CL core spots have Eu/Eu* of 0.07–0.60 (average 0.28) and Ce/Ce* of 1.89–24.27 (average 10.03). Because the contents of La and Pr are typically very low, Ce* in this study is obtained by the formulation $(Nd_N)^2 / Sm_N$ (Loader et al., 2017). The dark-CL rim spots have Eu/Eu* of 0.08–0.24 (average 0.13) and Ce/Ce* of 6.57–200.31 (average 79.23). These results indicate that the light-CL core has a weaker negative Eu anomaly and a weaker positive Ce anomaly than the dark-CL rim. The inherited zircon spots have ΣREE of 602–1517 ppm and show depletion of LREE, enrichment of HREE, a positive Ce anomaly (Ce/Ce* of 1.52–216.08), and a negative Eu anomaly (Eu/Eu* of 0.07–0.13) (Fig. 6c).

5.3 Zircon U–Pb and Hf isotope composition

A total of 77 spots were analyzed for U–Pb isotope composition from samples XY-001 and XY-008. In the U–Pb concordia diagram (Fig. 7a, c), both the light-CL core and dark-CL rim spots overlap within uncertainty on the concordia curve. There is a large degree of overlap between the 29 spots of the dark-CL rim and 32 spots of the light-CL core in terms of $^{206}Pb/^{238}U$ age, although the average value for $^{206}Pb/^{238}U$ age is higher in the 32 spots of the light-CL core

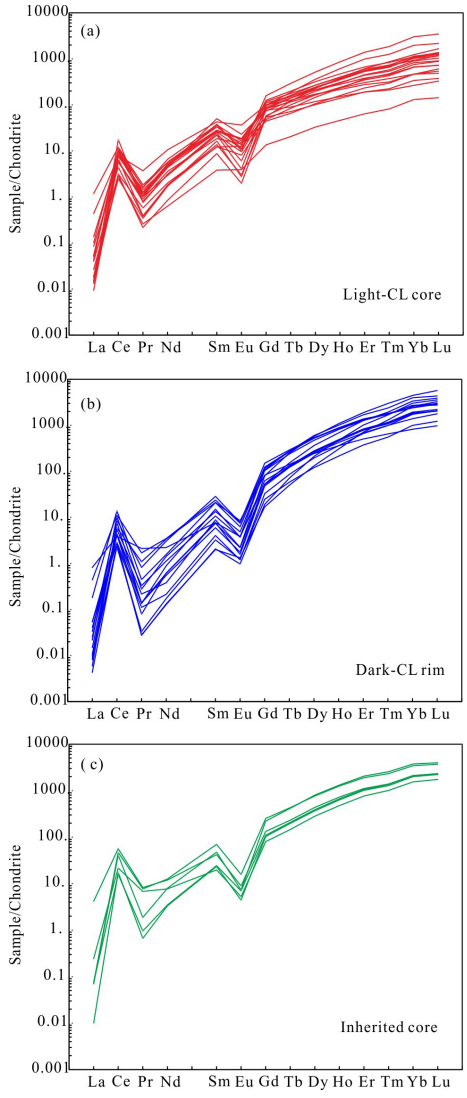

Figure 6. Chondrite-normalized REE patterns of zircon (chondrite values are from Sun and McDonough, 1989).

(Fig. 7e). On a single zircon, the $^{206}Pb/^{238}U$ age of the light-CL core is older than that of the dark-CL rim (Fig. 5), but the two values are within the error range of the in situ LA-ICP-MS analyses (individual spot of ± 3 %–5 % relative precision, Schmitz and Kuiper, 2013). In sample XY-001, 33 spots define a weighted mean $^{206}Pb/^{238}U$ age of 160.7 ± 1.1 Ma (2σ, MSWD = 1.3; Fig. 7b). In sample XY-008, 28 spots define a weighted mean $^{206}Pb/^{238}U$ age of 159.6 ± 1.1 Ma (2σ, MSWD = 1.2; Fig. 7d). The other 10 spots with distinctly older ages ($^{207}Pb/^{206}Pb$ ages ranging from 2500 to 2173 Ma) were obtained on inherited cores. Their ages are discordant, suggesting that these inherited cores were variably influenced by lead loss. Among these, nine spots define a discordia line with an upper intercept age of 2163 ± 13 Ma (MSWD = 0.45) (Fig. 7f).

A total of 24 zircons were analyzed for Lu–Hf isotope composition. The variation in Hf isotopic data is limited: between nine spots from the light-CL core and nine spots from the dark-CL rim. A total of 18 spots exhibit a range of $^{176}Hf/^{177}Hf$ ratios from 0.281921 to 0.282030, which converts to $\varepsilon Hf(t)$ values between −26.6 and −22.8 (Fig. 8), and two-stage Hf model (T_{DM2}) ages of 2650 to 2889 Ma by using the U–Pb age for each zircon. Six analytical spots, which define the concordia upper intercept age of 2163 Ma, show $^{176}Hf/^{177}Hf$ ratios and $\varepsilon Hf(t)$ values of 0.281443 to 0.281496 and −0.7 to 1.5, respectively, with T_{DM2} age of 2648 to 2791 Ma by using the upper intercept age.

6 Discussion

6.1 Significance of the two stages of zircon

Generally, zircon with high U content can easily break down into the metamict state because of the radiation damage to the lattice caused by α particles originating from the decay of uranium (Mezger and Krogstad, 1997). The physical and structural changes often lead to the loss of Pb and addition of trace elements such as LREEs. In this study, the dark-CL rim spots have high U content, which is significantly higher than the median value of zircon U content in granitic magma (350 ppm, Wang et al., 2011). Hence, the metamictization degree of the zircons must be taken into consideration. Data from dark-CL rim spots plot on the concordia curve, indicating no obvious Pb loss. The internal structure of the dark-CL rim is relatively intact, with obvious oscillatory zoning and few cracks, implying that the physical and structural nature of the dark-CL rim remained unchanged. Nasdala et al. (1998) suggested that the metamictization of zircon can be well characterized by Raman spectroscopy. The half-widths of the $\upsilon_3(SiO_4)$ Raman band (b) of 10 and 20 cm^{-1} are proposed to approximately distinguish well-crystallized, intermediate, and metamict zircons (Nasdala et al., 1998). The dark-CL rim has b values of 5.4–9.2, characterizing is as well-crystallized. Therefore, the above features indicate that the dark-CL rim is not metamict. Consequently, it can be concluded that the U–Pb isotope and trace element systematics of the dark-CL rim have not been changed by metamictization.

Both the light-CL core and dark-CL rim have oscillatory zoning patterns, and their chondrite-normalized REE patterns are characterized by steeply positive slopes from the LREE to HREE with strong negative Eu anomalies and pronounced positive Ce anomalies. The above characteristics are consistent with those of igneous zircon (Hoskin and Schaltegger, 2003). Although hydrothermal zircon can also have oscillatory zoning patterns similar to magmatic zircons, there are obvious differences in trace elements between the magmatic and hydrothermal zircon (Hoskin, 2005). In the discrimination diagram (Fig. 9), the spots of both the

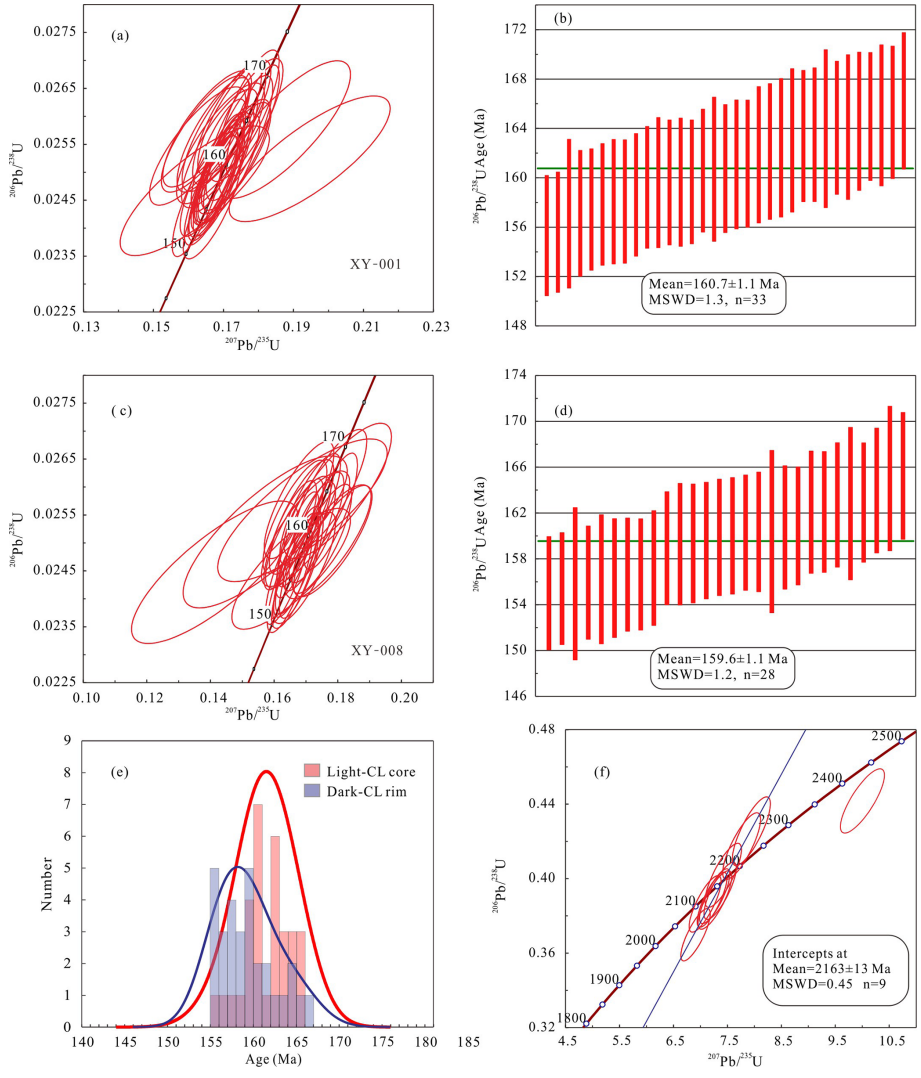

Figure 7. Concordia diagrams for zircon LA-ICP-MS U–Pb analyses.

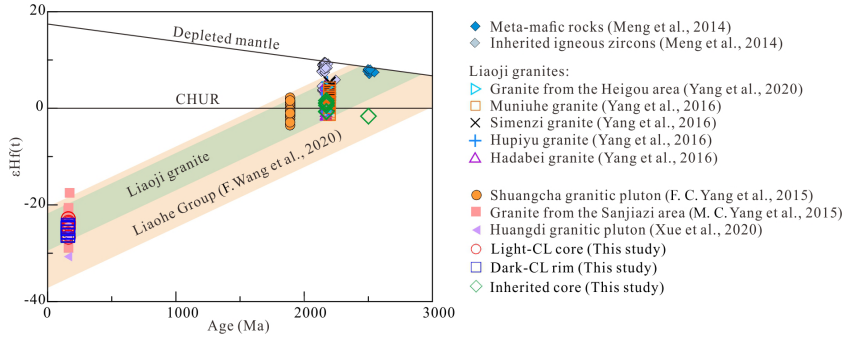

Figure 8. Zircon εHf(t) age (Ma) diagram for samples in this study and published data for the region.

light-CL core and dark-CL rim fall in or near the magmatic field, which is obviously different from hydrothermal zircon. Hence, the above characteristics indicate that both the light-CL core and dark-CL rim have a magmatic origin.

The light-CL core was overgrown continuously by the dark-CL rim. In addition, the contact between the light-CL core and dark-CL rim is euhedral. Such core–mantle overgrowth relationships indicate that the light-CL core domains are not inherited zircons. The similar Hf isotopic data for the light-CL core and dark-CL rim are also consistent with this interpretation. For the age population, samples XY-001 and XY-008 have MSWD of 1.3 and 1.2, respectively, which are both within the expected range for the 95 % confidence interval (Mahon, 1996). Although the $^{206}Pb/^{238}U$ age of the dark-CL rim is generally younger than that of the light-CL core, the ages of these two distinct domains have the characteristics of continuous variation and do not show two or more distinct age populations (Fig. 7b, d). These phenomena do not support the presence of antecrystic zircons (Siégel et al., 2018). Hence, both the light-CL core and dark-CL rim are most likely autocrystic zircon formed in one distinct pulse of magma. The weighted mean U–Pb ages of 160.7 ± 1.1 and 159.6 ± 1.1 Ma can be interpreted as the emplacement age of the Zhoujiapuzi granite. The obvious difference in internal structure and trace element composition between the light-CL core and dark-CL rim could be due to significant changes in their crystallization environments (Wang et al., 2007).

The Zr/Hf ratio in zircon has a negative correlation with the degree of fractionation in the parent melt (Claiborne et al., 2006). In this study, the Zr/Hf ratios of the dark-CL rim (21–40) are obviously lower than those of the light-CL core (39–56) (Fig. 10a). In addition, incompatible elements such as U and REEs will become enriched in the highly evolved magma (Zhao et al., 2014). In this study, the contents of U and REEs of the dark-CL rim are significantly higher than those of the light-CL core (Fig. 10a). Overall, the above features reflect the fact that the dark-CL rim crystallized from a later and more evolved magma.

Watson and Harrison (2005) found that the Ti content of zircon has a strong dependence on temperature (T) and obtained a Ti-in-zircon thermometer ($T_{Zr–Ti}$). Since then, Ferry and Watson (2007) suggested that the solubility of Ti in zircon depends not only on T and activity of TiO_2 ($aTiO_2$), but also on the activity of SiO_2 ($aSiO_2$), and revised the $T_{Zr–Ti}$. We use the $T_{Zr–Ti}$ from Ferry and Watson (2007) and the recommended values ($aSiO_2 = 1$, $aTiO_2 = 0.5$) for the activity of SiO_2 and TiO_2 (Schiller and Finger, 2019) due to the presence of ilmenite and quartz in the Zhoujiapuzi granite. The $T_{Zr–Ti}$ values from the light-CL core and dark-CL rim are 684–830° (average 761°) and 509–712° (average 635°), respectively; i.e., the light-CL core formed at higher temperatures than the dark-CL rim. The $T_{Zr–Ti}$ value shows a significant positive correlation with Zr/Hf (a tracer of fractional crystallization) and shows continual fractionation and cooling (Fig. 10b). As the light-CL core and dark-CL rim formed in different magmatic evolution stages, it is problematic to use the same $aSiO_2$ and $aTiO_2$ values to calculate $T_{Zr–Ti}$ values for both. For ilmenite-bearing granites, Schiller and Finger (2019) suggested that the variation of $aTiO_2$ values corresponding to different zircon crystallization stages is small. In addition, Schiller and Finger (2019) showed that the $aSiO_2$ value of the ilmenite-bearing granites at the onset of magmatic zircon crystallization was more than 0.75. Even if the $aSiO_2$ value of the light-CL core is changed from 1.0 to 0.75, the temperature will only drop by about $\sim 27°$, which is significantly lower than the 126° difference between the average $T_{Zr–Ti}$ value of the light-CL core and dark-CL rim. Therefore, it is certain that the light-CL core formed at higher temperatures than the dark-CL rim, although we cannot calculate the specific temperature difference.

Cerium exists in magmas as both Ce^{3+} and Ce^{4+}. Because the 0.84 Å radius of the Zr^{4+} ion is more closely matched by the Ce^{4+} (0.97 Å radius) than the Ce^{3+} (1.143 Å radius) (all ionic radii are from Shannon, 1976), Ce^{4+} is more compatible in the zircon structure than the Ce^{3+}. Hence, the magnitude of the Ce anomaly is a useful tool for evaluating the oxygen fugacity condition of a crystallization environment (e.g., Ballard et al., 2002; Trail et al., 2012). Loader et al. (2017) suggested that the Ce/Ce^* ratio is likely to be the most robust measure of magma redox conditions, although it is only a semi-quantitative measure. In this study, the Ce/Ce^* ratios of the light-CL core and dark-CL rim are 6.30–153.36 (average 32.51) and 21.81–5773.06 (average 787.39), respectively. This result suggests that the dark-CL rim formed in a higher-oxygen-fugacity environment than the light-CL core. As shown in the Ce/Ce^*-Zr/Hf diagram (Fig. 10c), Ce/Ce^* has a significant negative correlation with Zr/Hf, showing that the oxygen fugacity condition increases with the evolution of magma.

The absence of enclaves and disequilibrium textures in the Zhoujiapuzi granite and uniform $\varepsilon Hf(t)$ values of the light-CL core and dark-CL rim do not support magma mixing and wall-rock assimilation. Consequently, the abrupt change between the crystallization environment of the light-CL core and dark-CL rim is not due to magma mixing or contamination during magma evolution. Therefore, we propose that the light-CL core was formed in a relatively deep magma chamber, which had low oxygen fugacity, low Zr saturation, and higher temperature. The low Th, U, and REEs, as well as widely spaced oscillatory zoning patterns, indicate a low growth rate of zircon (Hoskin and Schaltegger, 2003; Wang et al., 2011). In contrast, the dark-CL rim was formed during the ascent and/or at the emplacement location of the magma. At this stage, the oxygen fugacity significantly increased, the temperature decreased, and Zr saturation increased due to the crystallization differentiation. In this environment, the crystallization rate of zircon significantly increased, forming the zircons with a higher content of Th, U, and REEs, low CL emission, and narrowly spaced oscillatory zoning patterns.

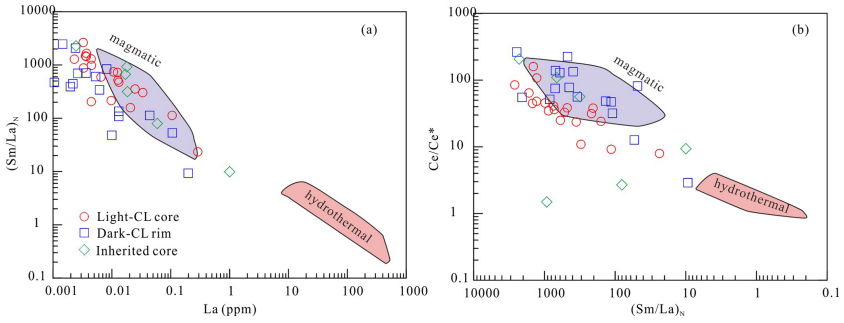

Figure 9. Discrimination plots for magmatic and hydrothermal zircon (Hoskin, 2005).

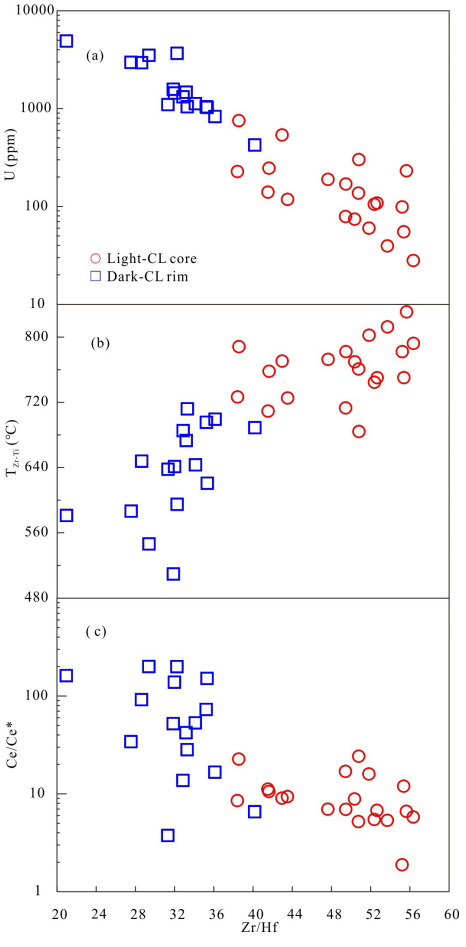

Figure 10. Covariation diagrams for zircon from the Zhoujiapuzi granite. **(a)** U vs. Zr/Hf; **(b)** $T_{Zr–Ti}$ vs. Zr/Hf; **(c)** Ce/Ce* vs. Zr/Hf.

Zircon U–Pb dating is the most commonly used method in geochronology, especially dating the emplacement age of magmatic rocks. A weighted mean age or upper intercept age is usually obtained to represent the emplacement time of a magmatic rock. However, the autocrystic zircons in this study record two different magmatic evolution stages. Previous studies, such as Wang et al. (2007), Zhao et al. (2014), and Chen et al. (2020), also show that zircons can crystallize continually or intermittently in a single phase of magmatism, showing several growth zones of clearly different internal structure and distinct time difference. Therefore, autocrystic zircon can be formed in two or more evolution stages during one distinct pulse or increment of magma. Some scholars even consider the possibility that the age difference of different stages can be more than dozens of millions of years (Wang et al., 2007). Therefore, if the zircon ages in the same magmatic rock have a large range of variation, this could be caused by the zircons recording different stages in magmatic evolution related to different levels of magma within the crust and/or different temperature regimes. In this paper, although the apparent age of the dark-CL rim is generally younger than that of the light-CL core, the age difference between the two is within the error range of the in situ LA-ICP-MS analyses (individual spot of ± 3 %–5 % relative precision). Therefore, further work is needed to verify the actual age difference between the two magmatic evolution stages. Nevertheless, it is notable that the bulk petrology and geochemistry of the host pluton do not record and reveal this two-stage magmatic evolution, which can only be detected in the zircon analysis.

6.2 Genetic type: I-type affinity

The Zhoujiapuzi granite has low Zr (113–242 ppm), Ce (26.5–121.5 ppm), Zr + Nb + Ce + Y (152.0–382.6 ppm), $(Na_2O + K_2O) / CaO$ (4.53–8.31), and FeO^*/MgO (5.09–10.56), distinct from the typical A-type granites (Fig. 11a–d). Furthermore, the Zhoujiapuzi granite does not contain mafic alkaline minerals, such as arfvedsonite and riebeckite, which is also distinctly inconsistent with typical A-type granites (Wu et al., 2003). Wu et al. (2017) suggested that a high formation temperature is one of the most important characteristics of A-type granite. Zircon saturation thermometry (T_{Zrn}) and a Ti-in-zircon thermometer ($T_{Zr–Ti}$) are two methods for estimating magma temperatures. As noted above, because the values of $aSiO_2$ and $aTiO_2$ during the early zircon crystallization cannot be accurately obtained, the temperature of this period cannot be accurately obtained through the Ti-in-zircon thermometer. Zircon saturation thermome-

try was introduced by Watson and Harrison (1983) and is suitable for non-peralkaline crustal source rocks. Since the zircon solubility is mainly affected by temperature, major element compositions have a limited impact on calculated T_{Zrn} (Miller et al., 2003). In addition, the errors introduced by crystal-rich composition tend to cancel as changes in Zr concentration and M value during crystallization have opposite effects on the T_{Zrn} value (Miller et al., 2003). Therefore, the composition of Zhoujiapuzi granite can be used to estimate the magma temperature. The calculated TZrn values for the Zhoujiapuzi granite are in the range of 803–870 °C (mean = 845 ± 20 °C). It was proposed that the T_{Zrn} suggests an upper limit on the temperature of melt generation for inheritance-rich granitoid (Miller et al., 2003). Hence, the magma temperature of the Zhoujiapuzi granite should be lower than or equal to the T_{Zrn} value, which is significantly lower than that of typical A-type granite (> 900°, Skjerlie and Johnston, 1992; Douce, 1997). Thus, the Zhoujiapuzi granite is not an A-type granite.

The samples of the Zhoujiapuzi granite have A/KNC < 1.1, have relatively high Na_2O (3.96 wt %–4.65 wt %), and lack peraluminous minerals (e.g., cordierite, andalusite, muscovite, and garnet), which are clearly different from S-type granites (Chappell and White, 1992). With the rise of the degree of crystallization, P_2O_5 contents (generally > 0.1 wt %) increase in S-type granites, accompanied by an increase and/or immutability in SiO_2 (Wolf and London, 1994). However, the Zhoujiapuzi granite samples have low P_2O_5 contents (0.02 wt %–0.08 wt %) and decrease with increasing SiO_2 (Fig. 11e), which are features consistent with I-type granite rather than S-type granite (Chappell and White, 1992). Additionally, Rb has a positive correlation with Y (Fig. 11f), which has been considered an indicator of I-type granite (Jiang et al., 2018). Furthermore, the composition of the Zhoujiapuzi granite falls in the I-type granite field in the discrimination diagrams of granites introduced by Collins et al. (1982) (Fig. 11c–d). Therefore, we conclude that the Zhoujiapuzi granite is an I-type granite.

6.3 Petrogenesis of the high-Sr/Y granite

The samples of the Zhoujiapuzi granite have high Sr/Y and $(La/Yb)_N$ ratios and low Y and Yb contents (Fig. 12a) consistent with the geochemical signatures of modern adakites (Defant and Drummond, 1990). However, other geochemical parameters of the Zhoujiapuzi granite, such as the high K_2O/Na_2O ratio (0.93–1.22), low Al_2O_3 content (14.49 %–15.02 %, except one) and Sr content (in half of the samples lower than 400 ppm), are obviously different from typical adakites ($K_2O/Na_2O \leq 0.42$, $Al_2O_3 \geq 15$ %, Sr > 400 ppm, Defant and Drummond, 1990; Drummond et al., 1996; Martin et al., 2005). A variety of petrogenetic models have been proposed for the origin of high-Sr/Y magmatic rocks, such as partial melting of subducting oceanic crust (Model A, Defant and Drummond, 1990), delaminated lower continental crust (LCC) (Model B, Kay and Kay, 1993; Xu et al., 2002), differentiation of basaltic arc magma (Model C, Castillo et al., 1999), magma mixing between mantle-derived mafic and crust-derived silicic magmas (Model D, X. H. Ma et al., 2013), partial melting of thickened basaltic LCC (Model E, Gao et al., 2004; Ou et al., 2017), or melting of a high-Sr/Y (and La/Yb) source (Model F, Kamei et al., 2009; Ma et al., 2015).

6.3.1 Model A: partial melting of subducting oceanic crust

The partial melting of the young, hot, and hydrated subducted oceanic slab in the garnet stability field is the classical formation model of adakite (high-Sr/Y rock) (Defant and Drummond, 1990). Studies have shown that the rock with this genetic model generally has the characteristics of high mantle components (such as MgO, CaO, and Cr) because of the involvement of mantle magma (Wang et al., 2018). However, this phenomenon was not seen in the Zhoujiapuzi granite. In addition, the Zhoujiapuzi granite has high K_2O/Na_2O ratios (0.92–1.22, average 1.13), which is inconsistent with the slab-derived adakites ($K_2O/Na_2O = \sim 0.4$, Martin et al., 2005). Moreover, the low $\varepsilon Hf(t)$ values (−26.6 to −22.8) of the Zhoujiapuzi granite are also inconsistent with the magmas derived from the partial melting of oceanic crust, which generally have a depleted isotopic character (Zhan et al., 2020). Furthermore, the Zhoujiapuzi granite has low Ti/Eu and high Nd/Sm ratios (Fig. 13a), as well as markedly negative Nb–Ta anomalies (Fig. 4b), which are distinct from those of oceanic basalts (Yu et al., 2012). In summary, the Zhoujiapuzi granite is difficult to explain by Model A.

6.3.2 Model B: delaminated lower continental crust (LCC)

High-density, garnet-bearing mafic lower crust delaminating or foundering into the asthenosphere mantle and subsequent interaction with mantle peridotite could produce high-Sr/Y magmas (Kay and Kay, 1993). Because the melt formed by partial melting of the delaminated lower crust would interact with mantle peridotite during magma ascent, the high-Sr/Y magmas related to this petrogenetic model generally have high MgO, Mg#, and TiO_2 (Gao et al., 2004; Ou et al., 2017; He et al., 2021). The MgO (0.10 wt %–0.44 wt %), Mg# (15–26), and TiO_2 (0.09 wt %–0.34 wt %) values of Zhoujiapuzi granite are significantly lower than the above values (Fig. 13b–d). In addition, delamination of the lower crust generally occurs in within-plate extensional settings (Gao et al., 2004) and will form a large number of Mg-rich (Mg# > 50) rocks due to the partial melting of lithospheric mantle and/or upwelling of asthenosphere (Ou et al., 2017). However, these Jurassic magmatic rocks in the Liaodong Peninsula are generally considered to have been formed in a compressional environment related to the subduction of the

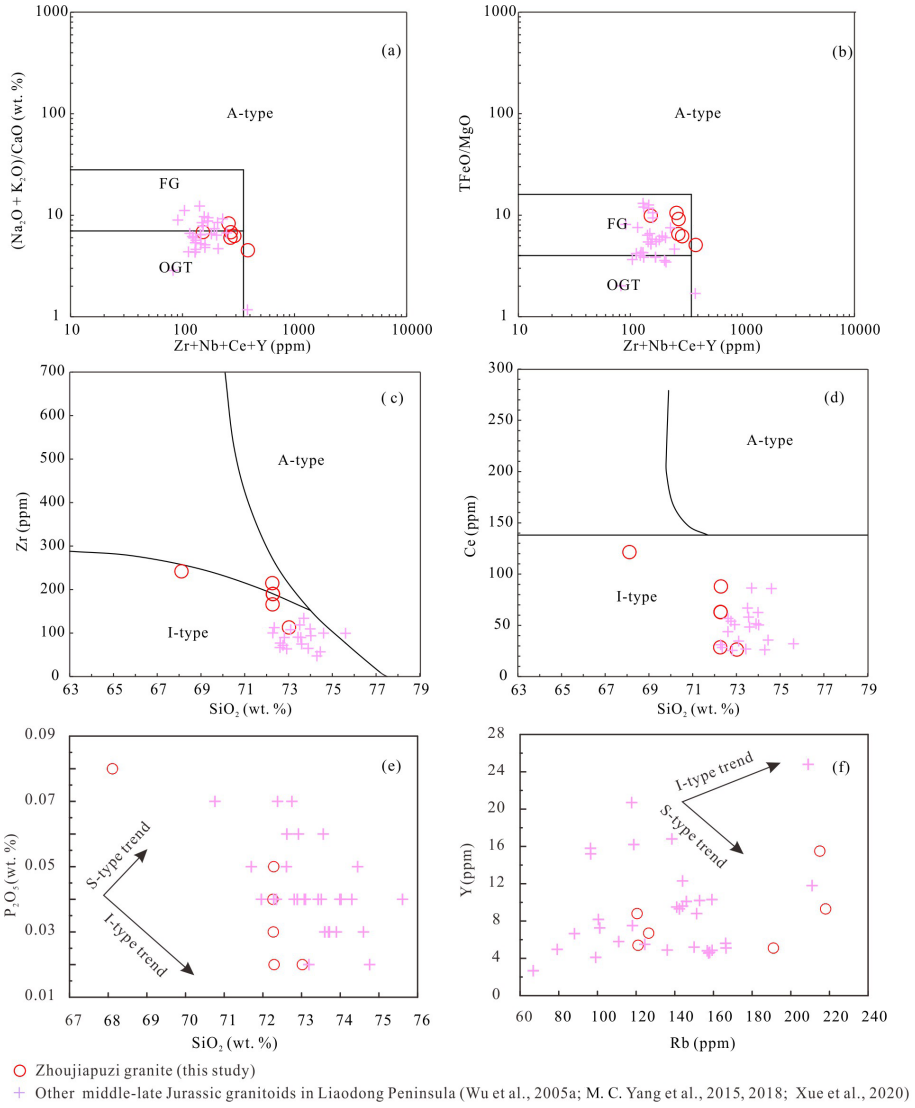

Figure 11. Chemical variation diagrams for the Zhoujiapuzi granite. **(a, b)** Zr + Nb + Ce + Y vs. $(Na_2O + K_2O) / CaO$ and TFeO/MgO (after Whalen et al., 1987); **(c, d)** SiO_2 vs. Zr and Ce (after Collins et al., 1982); **(e)** SiO_2 vs. P_2O_5 diagram; **(f)** Rb vs. Y diagram.

Paleo-Pacific slab (Li et al., 2004; F. C. Yang et al., 2015; Zhu and Xu, 2019; Zheng et al., 2018). Furthermore, the Middle–Late Jurassic granites are generally Mg-poor (Fig. 13c). Due to the high temperature of the asthenosphere (1200°, Parsons and McKenzie, 1978; King et al., 2015), rocks formed by partial melting of the delaminated lower crust should possess a high-temperature fingerprint. T_{Zrn} has been used as a geothermometer to estimate partial melting temperatures (e.g., Miller et al., 2003; Collins et al., 2016). As mentioned before, the T_{Zrn} of the Zhoujiapuzi granite is below 900°, which is markedly lower than the temperature of the asthenosphere. Therefore, the petrogenetic model of delaminated lower continental crust (Model B) is also inconsistent with the Zhoujiapuzi granite.

6.3.3 Model C: differentiation of basaltic arc magma

Low-pressure fractional crystallization (involving olivine + clinopyroxene + plagioclase + amphibole + titanomagnetite) and high-pressure fractional crystallization (involving garnet) from basaltic magmas have been proposed as two ways to generate adakitic characteristics (Castillo et al., 1999; Macpherson et al., 2006).

However, the composition of the Zhoujiapuzi granite is relatively uniform, including SiO_2, MgO, and Na_2O, which does not support major fractional crystallization (Xue et al., 2017). Furthermore, the Zhoujiapuzi granite has abundant inherited zircons and no obvious depletion of Sr, Eu, and Ba, showing that this granite has not experienced extensive fractionation (Miller et al., 2003). The samples form clear partial melting trends on the La/Yb versus La diagram (Fig. 13e),

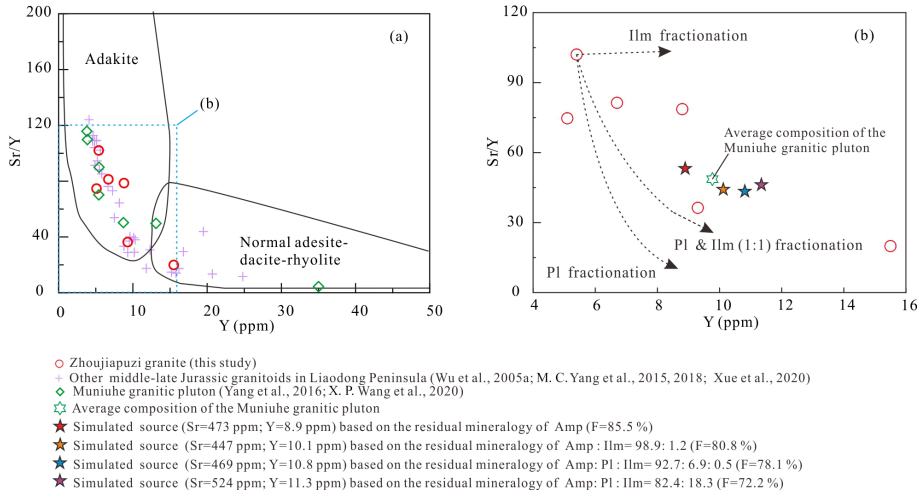

Figure 12. Adakite discrimination diagrams for the Zhoujiapuzi granite (after Defant and Drummond, 1990).

which also suggests that partial melting was more important than fractional crystallization (Gao et al., 2007; Shahbazi et al., 2021). In addition, crystal fractionation of basaltic melts can only form minor volumes of granitic melts; the ratio of the two is about 9 : 1 (Zeng et al., 2016). However, for the same age interval, no coexisting mafic-intermediate rocks have been found in the research area. In the wider region of the Liaodong Peninsula, Middle–Late Jurassic magmatism is dominated by felsic compositions; mafic-intermediate rocks are only reported in the Huaziyu area (lamprophyre dikes, Jiang et al., 2005). Therefore, it is unlikely that there are large-scale mafic-intermediate rocks contemporaneous with the Zhoujiapuzi granite at depth according to the rock assemblage of the Liaodong Peninsula in this period. Moreover, the zircon Hf isotopic compositions of the Zhoujiapuzi granite are quite different from those of the depleted mantle but are similar to those of the basement (Liaohe Group and Liaoji granite) in the study area (Fig. 8). The ancient inherited zircons (2500 to 2173) with low $\varepsilon Hf(t)$ values also indicate older crustal material in the Zhoujiapuzi granite. For these reasons, it is highly improbable that Zhoujiapuzi granite was derived by differentiation of basaltic magma (Model C).

6.3.4 Model D: magma mixing between mantle-derived mafic and crust-derived silicic magmas

The Zhoujiapuzi granite has a high K_2O/Na_2O ratio (> 1) and A/CNK value (> 1), together with the absence of mingling textures, mafic microgranular enclaves (MMEs), felsic xenocrysts, and melting texture of plagioclase, implying that the mantle-derived magma is unlikely to have played an important role in the genesis of the Zhoujiapuzi granite (Castro et al., 1991). In addition, the Zhoujiapuzi granite is characterized by the development of biotite but lacks amphibole and pyroxene. These features, coupled with the high A/CNK value, are consistent with an origin as a crust-derived granitoid, but obviously different from the granitoids formed by crust–mantle-derived magma mixing (Barbarin, 1990). Moreover, granites formed by magma mixing generally have high MgO, TFe_2O_3, CaO, and Cr contents and low SiO_2 content (X. H. Ma et al., 2013; Wang et al., 2018). These features are obviously inconsistent with the Zhoujiapuzi granite in this study. Additionally, the $\varepsilon Hf(t)$ values and trace element composition of the two stages of zircon also do not support magma mixing. Hence, magma mixing of mantle-derived and crust-derived magmas (Model D) is also unlikely to have produced the Zhoujiapuzi granite.

6.3.5 Model E: partial melting of thickened basaltic LCC

Experimental studies have shown that the partial melt of basaltic LCC in the garnet stabilization zone (> 40 km, i.e., ~ 1.2 GPa) can produce magma with a high Sr/Y ratio (Rapp et al., 2003, and references therein). In these scenarios, high Sr/Y and overall adakitic affinity are caused by leaving garnet as residual phases (e.g., Gao et al., 2004). Based on geochemical data for the Zhoujiapuzi granites, partial melting of thickened basaltic LCC is also unlikely to account for the high-Sr/Y Zhoujiapuzi granite (Model E). This conclusion is based on the following observations.

1. This ratio of $(Gd/Yb)_N$ is the most important feature to judge whether garnet is involved in magma genesis (Ma et al., 2012). If the $(Gd/Yb)_N$ ratio of the source is similar to the average value of the LCC (1.71, Rudnick and Gao, 2003), partial melting of these crustal materials controlled by garnet at high pressure can produce melt with $(Gd/Yb)_N$ of 5.8 (Huang and He, 2010). In contrast, the $(Gd/Yb)_N$ values (1.22–5.06, average 2.69) of the Zhoujiapuzi granite are relatively low.

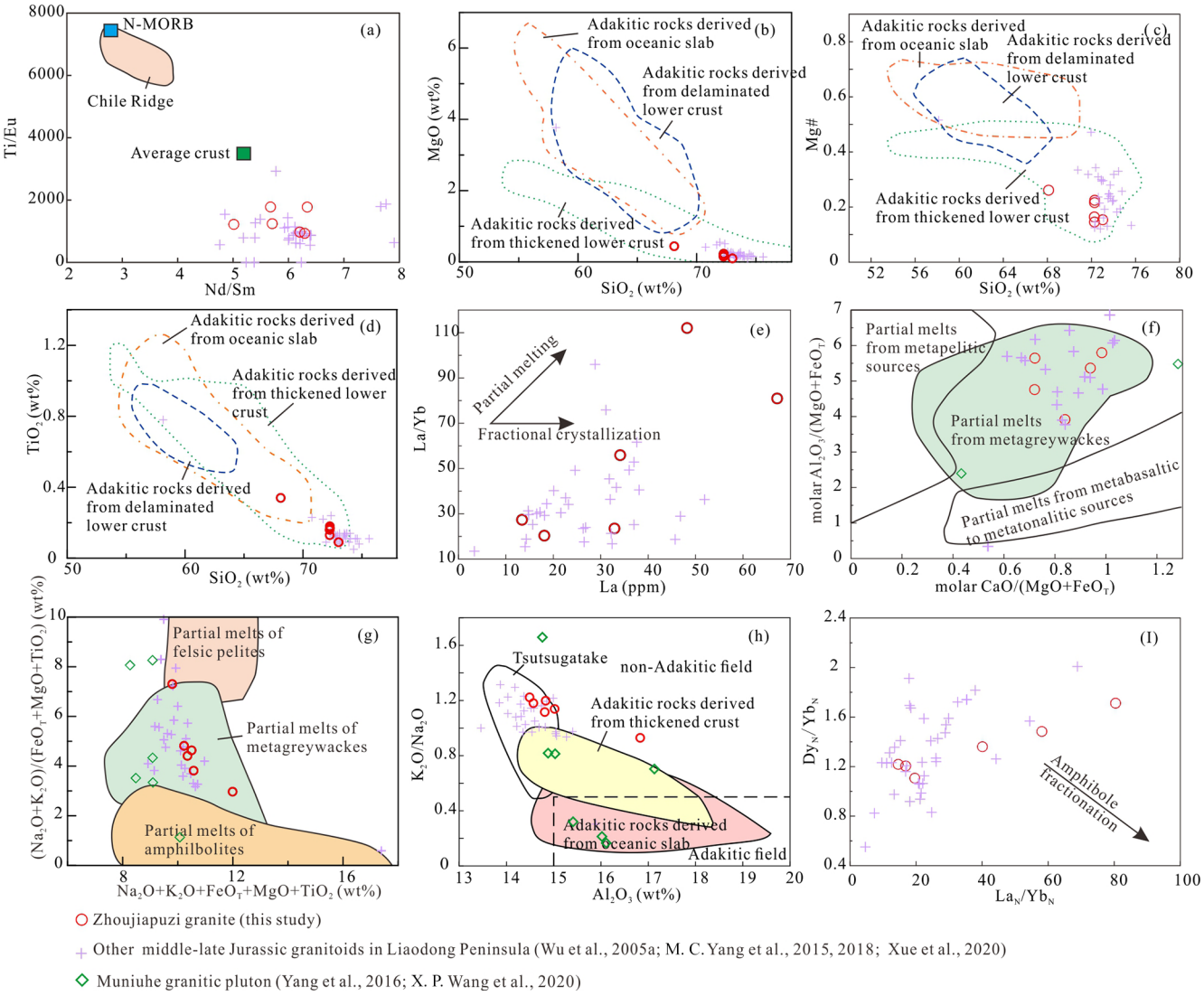

Figure 13. Source characteristics (**a–d**, **f–h**) and crystal fractionation **(e, i)** discrimination diagrams for the Zhoujiapuzi granite. **(a)** Nd/Sm vs. Ti/Eu (Yu et al., 2012); **(b–d)** SiO_2 vs. MgO, Mg#, and TiO_2 (after Wang et al., 2006); **(e)** La vs. La/Yb (Gao et al., 2007); **(f)** molar Al_2O_3 / $(MgO + FeO_T)$ vs. molar CaO / $(MgO + FeO_T)$ (after Altherr et al., 2000); **(g)** $(Na_2O + K_2O)$ / $(FeO_T + MgO + TiO_2)$ vs. $Na_2O + K_2O + FeO_T + MgO + TiO_2$ (after Patiño Douce, 1999); **(h)** K_2O/Na_2O vs. Al_2O_3 diagrams (after Kamei et al., 2009); **(i)** La_N/Yb_N vs. Dy_N/Yb_N.

2. Studies of lower-crustal xenoliths show that garnet may not be a common mineral in the lower crust of the NCC (Ma et al., 2012).

3. As shown in the discrimination diagrams of granite sources (Fig. 13f, g), all samples fall in the range of metagraywacke-derived melts. Therefore, the Zhoujiapuzi granite was considered to have been derived from crustal anatexis of metagraywacke (or intermediate-acid igneous rock with similar mineral composition) rather than basaltic lower crust.

6.3.6 Model F: melting of a high-Sr/Y (and La/Yb) source

Studies have shown that when a source rock has a high Sr/Y ratio, the high Sr/Y signature of the derived magma can be inherited from the source, regardless of pressure (Kamei et al., 2009; Moyen, 2009; Ma et al., 2015). We suggest that partial melting of high-Sr/Y Liaoji granite was most probably the origin of the high-Sr/Y Zhoujiapuzi granite, as discussed below (Model F).

The Zhoujiapuzi granite has similar mineral assemblages (contains abundant K-feldspar and lacks hornblende) and geochemical composition (Fig. 13h) as the Tsutsugatake

intrusion, which is explained by partial melting of arc-type tonalite or adakitic granodiorite (Kamei et al., 2009). Among the inherited zircons from Zhoujiapuzi granite, the $^{207}Pb/^{206}Pb$ ages of all the spots are between 2132 and 2200 Ma, except one, and yield a concordia upper intercept age of 2163 Ma. Both assimilation of country rocks and incomplete melting of source rocks can explain the genesis of inherited zircon in granite. Due to the similar T_{DM2} of autocrystic zircons (light-CL core and dark-CL rim) and inherited zircons, these inherited zircons most likely come from the source of the Zhoujiapuzi granite. In the study area, metasedimentary rocks and meta-volcanic rocks of the South Liaohe Group, Paleoproterozoic mafic rocks, and the Liaoji granites have ∼ 2.16 Ga zircon. In spite of an age peak of 2.17–2.16 Ga in detrital zircon age spectra of the metasediments from the South Liaohe Group, melting of a sediment-dominated source is unlikely to have occurred, as it would have also introduced other age peaks such as ∼ 2.03 and ∼ 2.50 Ga (Li et al., 2015; F. Wang et al., 2020). In addition, given the I-type characteristics of the Zhoujiapuzi granite, derivation from an igneous precursor is more plausible than a metasedimentary origin (Chappell and White, 1992). Therefore, these ∼ 2.16 Ga zircons from the Zhoujiapuzi granite are unlikely to have come from the South Liaohe Group. As shown in the host rock discrimination diagrams (Fig. 14, introduced by Belousova et al., 2002), all the ∼ 2.16 Ga inherited zircons from Zhoujiapuzi granite fall into the granitoid area (Fig. 14), precluding the idea that these ∼ 2.16 Ga zircons come from the Paleoproterozoic mafic rocks. In addition, the ∼ 2.16 Ga inherited zircons from Zhoujiapuzi granite and the zircons from the Liaoji granites lie in a similar area in the $\varepsilon Hf(t)$ age (Ma) diagram (Fig. 8). Hence, the ∼ 2.16 Ga inherited zircon most likely comes from the Liaoji granites.

Some of the Liaoji granites, such as the Muniuhe granite (comprising granodiorite and syenogranite with no distinct boundary between the two), have adakitic signatures as well as similar REE and trace element patterns as the Zhoujiapuzi granite (Fig. 4). Based on a model of batch melting (Shaw, 1970) using the experiments of Conrad et al. (1988), the high-Sr/Y characteristic of the Zhoujiapuzi granite can be explained by partial melting of Muniuhe granitic pluton leaving amphibole as the main residue (Fig. 12b).

In our modeling, we choose the XY-005 sample to approximately represent the primitive melt composition for the following reasons. As mentioned above, the high-Sr/Y characteristics of the Zhoujiapuzi granite are not caused by the fractional crystallization of amphibole. Furthermore, the lack of positive correlation between Dy_N/Yb_N ratios and La_N/Yb_N ratios (Fig. 13i) also suggests that fractional crystallization of amphibole was not a significant process for the Zhoujiapuzi granite. On the other hand, the samples of Zhoujiapuzi granite display variable Eu and Sr contents, implying that plagioclase is likely a fractional phase. The separation of titanomagnetite could explain the positive trend in TFe_2O_3 with increasing TiO_2 content, consistent with the occurrences of magnetite in some studied rocks. This possible mineral assemblage of fractional crystallization is also reflected by the chemical variations in the Sr/Y–Y diagram (Fig. 12b). Hence, sample XY-005, which has the highest Sr/Y, was chosen to represent a primitive melt composition. To find the best-matching experimental melts, we have compared the major elements of the XY-005 sample with those of experimental melts and the characteristics of no garnet residue discussed above. Results are shown in Fig. 12b. The Sr and Y compositions of the starting material used in these experiments resemble those of the average composition of the Muniuhe granitic pluton (Sr = 475 ppm, Y = 9.77 ppm) if the residue contains a large volume of amphibole (> 90 %). However, if more plagioclase is retained in the residue (e.g., 18.3 %), a source region with a higher Sr content is required. Therefore, a high-Sr/Y Liaoji granite similar to the Muniuhe granitic pluton can produce the high Sr/Y signatures of the Zhoujiapuzi granite.

A large number of Yanshanian adakites (or high-Sr/Y rocks) are developed in the NCC, which are generally considered to be derived from the thickened basaltic LCC (e.g., Gao et al., 2004; Wu et al., 2005a; L. Ma et al., 2013). Zhang et al. (2001, 2003) suggested that these so-called "C-type adakites" indicated a large-scale crustal thickening event. However, according to studies on the Triassic and Jurassic adakitic rocks near the Pingquan area in the northern part of the NCC, Ma et al. (2012, 2015) suggested that the adakitic signatures of these rocks are inherited from their source rocks. Research on the Zhoujiapuzi granite in this study also shows that among the widely distributed Jurassic high-Sr/Y granites in the Liaodong Peninsula, there is at least one pluton with a high Sr/Y signature inherited from the source. Therefore, we suggest that melting of a high-Sr/Y (and La/Yb) source is one of the important processes for the generation of Yanshanian high-Sr/Y rocks in the NCC. This kind of high-Sr/Y granite does not need to be formed in the garnet stability field.

6.4 Tectonic implications

A large number of Early Jurassic arc-like igneous rocks occur in the northeastern part of NCC–Korean Peninsula–Hida belt, which belong to the middle- to high-K calc–alkaline series and are characterized by enrichment in LILE and depletions in HFSE (Wu et al., 2007; Tang et al., 2018, and references therein). In addition, the Early Jurassic accretionary complexes in the eastern margin of the Eurasian continent and the Japan islands, such as the Heilongjiang complex, the Khabarovsk complex, and the Mino-Tamba complex, are considered to be related to subduction (Wu et al., 2007; Tang et al., 2018, and references therein). It is generally accepted that the Paleo-Pacific slab subducted westwards in the Early Jurassic (Tang et al., 2018; Zhu and Xu, 2019).

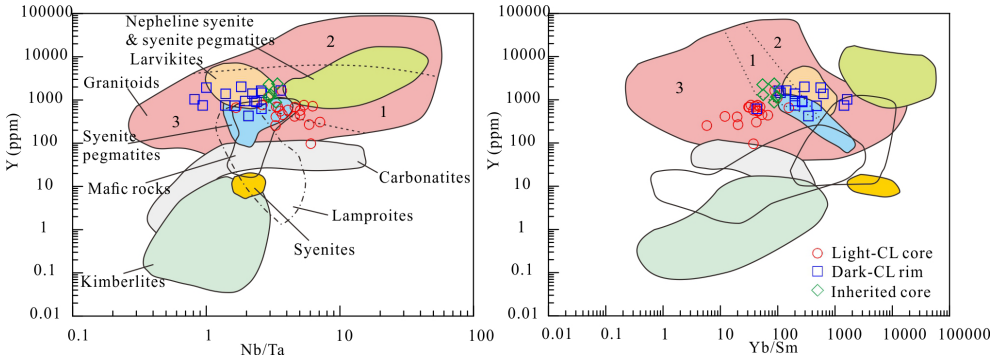

Figure 14. The fields of zircon compositions used as discriminants for different rock types (after Belousova et al., 2002). "Granitoids" include (1) aplites and leucogranites, (2) granites, and (3) granodiorites and tonalities.

In the Middle–Late Jurassic, I-type granites are dominant in the Liaodong Peninsula, such as the Zhoujiapuzi granite (this study), Heigou pluton, Gaoliduntai pluton (Wu et al., 2005a), Waling granite (F. C. Yang et al., 2015), and Wulong granite (Yang et al., 2018). There are no A-type granites, and mantle-derived magmatism is extremely rare. These granites were formed by partial melting of crustal materials without an obvious contribution of mantle-derived magma (Wu et al., 2005a; M. C. Yang et al., 2015; Yang et al., 2018; Xue et al., 2020). In addition, WNW–ESE compression during 157–143 Ma was widespread in the Liaodong Peninsula (Yang et al., 2004; Zhang et al., 2020). It not only mylonitized the granite plutons in middle–lower crust levels, but also intensely deformed the thick sedimentary cover in the upper crust (Qiu et al., 2018; Ren et al., 2020). Hence, Late Jurassic magmatism in the Liaodong Peninsula is most likely related to subduction of the Paleo-Pacific plate in a mature continental arc, with crust previously thickened by compressional tectonics, related to both the oceanic subduction and the earlier Mesozoic collisions at the northern and southern margins of the NCC. This setting would produce the conditions required for extensive crustal melting of pre-existing basement. There is a potential resemblance to the modern arc of the central Andes (Allmendinger et al., 1997), where crustal thickening and plateau growth developed over the Cenozoic (Scott et al., 2018), and melting of older basement took place during subduction of the Nazca plate (Miller and Harris, 1989). This model is also consistent with the idea that much of eastern China was a high orogenic plateau during the Mesozoic, before widespread Early Cretaceous extension and core complex development (Meng, 2003; Chu et al., 2020).

7 Conclusions

1. LA-ICP-MS zircon U–Pb dating indicates that the Zhoujiapuzi granite in the Liaodong Peninsula formed at ∼ 160 Ma.
2. Zircon growth in Zhoujiapuzi granite can be divided into two distinct stages. The light-CL core was formed in a deeper, hotter magma chamber, which had low oxygen fugacity and high temperature. The dark-CL rim formed from later, more evolved magma. Oxygen fugacity significantly increased and the temperature decreased at this stage. The Zhoujiapuzi granite is a case study of multistage generation and emplacement of magma revealed by zircons, with no signals discernible in the bulk petrology or geochemistry.
3. The I-type Zhoujiapuzi granite originated from partial melting of the Paleoproterozoic Liaoji granites. The high Sr/Y compositions are inherited from their source rocks rather than being a direct indication of deep crustal melting or any other common mechanism for generating adakitic signatures.
4. The Late Jurassic tectonic setting of the Liaodong Peninsula and the eastern NCC resembled the modern orogenic plateau of the central Andes, where silicic magmatism may occur by partial melting of older continental crust in a compressional environment, related to the subduction of the Paleo-Pacific plate.

Data availability. All the data presented in this paper are available upon request.

Supplement. The Supplement contains the table of major element (wt %) and trace element (ppm) compositions of the Zhoujiapuzi granite, Raman microprobe data, the zircon major elements (wt %), and trace elements (ppm) from the Zhoujiapuzi granite, as well as zircon La-ICP-MS U–Pb isotopic data with ages of the Zhoujiapuzi granite and zircon Hf isotopic data for the Zhoujiapuzi granite. The supplement related to this article is available online at: https://doi.org/10.5194/se-13-1259-2022-supplement.

Author contributions. RZ was responsible for fieldwork, conceptualization, methodology, and writing (original draft, review, and editing). MBA was responsible for conceptualization, supervision, and writing (review and editing). XM was responsible for funding acquisition and project administration. JL was responsible for funding acquisition and project administration. JY was responsible for review and editing. JW was responsible for laboratory analyses.

Competing interests. At least one of the (co-)authors is a member of the editorial board of *Solid Earth*. The peer-review process was guided by an independent editor, and the authors also have no other competing interests to declare.

Disclaimer. Publisher's note: Copernicus Publications remains neutral with regard to jurisdictional claims in published maps and institutional affiliations.

Acknowledgements. We thank Wenzhou Xiao, Jiajie Chen, and Quan Ou for constructive reviews and useful suggestions. We are also grateful to Ying Liu, Chunying Guo, Jianxiong Hu, and Ziming Hu for their help with the fieldwork.

Financial support. This research was funded by the National Nature Science Foundation of China (grant nos. 42030809, 41772349, 41902075, 42002095, and 42162013), the China Scholarship Council (grant no. 202008360018), the Geological Exploration Program of China Nuclear Geology (grant no. D1802), research grants from the East China University of Technology (grant no. DHBK2017103), and the Open Research Fund Program of the State Key Laboratory of Nuclear Resources and Environment (East China University of Technology) (grant no. 2020NRE13).

Review statement. This paper was edited by Johan Lissenberg and reviewed by Simon Large and one anonymous referee.

References

Allmendinger, R. W., Jordan, T. E., Kay, S. M., and Isacks, B. L.: The evolution of the Altiplano-Puna plateau of the Central Andes, Annu. Rev. Earth Pl. Sc., 25, 139–174, https://doi.org/10.1146/annurev.earth.25.1.139, 1997.

Altherr, R., Holl, A., Hegner, E., Langer, C., and Kreuzer, H.: High-potassium, calc-alkaline I-type plutonism in the European Variscides: northern Vosges (France) and northern Schwarzwald (Germany), Lithos, 50, 51–73, https://doi.org/10.1016/S0024-4937(99)00052-3, 2000.

Ballard, J. R., Palin, M. J., and Campbell, I. H.: Relative oxidation states of magmas inferred from Ce(IV)/Ce(III) in zircon: application to porphyry copper deposits of northern Chile, Contrib. Mineral. Petr., 144, 347–364, https://doi.org/10.1007/s00410-002-0402-5, 2002.

Barbarin, B.: Granitoids: main petrogenetic classifification in relation to origin and tectonic setting, Geol. J., 25, 227–238, 1990.

Belousova, E., Griffin, W., O'Reilly, S. Y., and Fisher, N.: Igneous zircon: trace element composition as an indicator of source rock type, Contrib. Mineral. Petr., 143, 602–622, https://doi.org/10.1007/s00410-002-0364-7, 2002.

Blichert-Toft, J. and Albarède, F.: The Lu-Hf isotope geochemistry of chondrites and the evolution of the mantle-crust system, Earth. Planet. Sc. Lett., 148, 243–258, https://doi.org/10.1016/S0012-821X(97)00040-X, 1997.

Breiter, K., Lamarão, C. N., Borges, R. M. K., and Dall'Agnol, R.: Chemical characteristics of zircon from A-type granites and comparison to zircon of S-type granites, Lithos, 192–195, 208–225, https://doi.org/10.1016/j.lithos.2014.02.004, 2014.

Castillo, P. R., Janney, P. E., and Solidum, R. U.: Petrology and geochemistry of Camiguin Island, southern Philippines: Insights to the source of adakites and other lavas in a complex arc setting, Contrib. Mineral. Petr., 134, 33–51, https://doi.org/10.1007/s004100050467, 1999.

Castro, A., Moreno-Ventas, I., and Rosa, J.: H-type (hybrid) granitoids: a proposed revision of the granite-type classification and nomenclature, Earth. Sci. Rev., 31, 237–253, https://doi.org/10.1016/0012-8252(91)90020-G, 1991.

Chappell, B. W. and White, A. J. R.: I-and S-type granites in the Lachlan Fold Belt, Geol. Soc. Am. Spec. Pap., 272, 1–26, https://doi.org/10.1130/SPE272-p1, 1992.

Chen, S. R., Wang, Q., Zhu, D. C., Weinberg, R. F., Zhang, L. L., and Zhao, Z. D.: Reheating and magma mixing recorded by zircon and quartz from high-silica rhyolite in the Coqen region, southern Tibet, Am. Mineral., 106, 112–122, https://doi.org/10.2138/am-2020-7426, 2020.

Chu, Y., Lin, W., Faure, M., Allen, M. B., and Feng, Z.: Cretaceous exhumation of the Triassic intracontinental Xuefengshan Belt: Delayed unroofing of an orogenic plateau across the South China Block?, Tectonophysics, 793, 228592, https://doi.org/10.1016/j.tecto.2020.228592, 2020.

Claiborne, L. L., Miller, C. F., Walker, B. A., Wooden, J. L., Mazdab, F. K., and Bea, F.: Tracking magmatic processes through Zr/Hf ratios in rocks and Hf and Ti zoning in zircons: An example from the Spirit Mountain batholith, Nevada, Mineral. Mag., 70, 517–543, https://doi.org/10.1180/0026461067050348, 2006.

Collins, W. J., Beams, S. D., White, A. J. R., and Chappell, B. W.: Nature and origin of A-type granites with particular reference to southeastern Australia, Contrib. Mineral. Petr., 80, 189–200, https://doi.org/10.1007/BF00374895, 1982.

Collins, W. J., Huang, H. Q., and Jiang, X. Y.: Water-fluxed crustal melting produces Cordilleran batholiths, Geology, 44, 143–146, https://doi.org/10.1130/G37398.1, 2016.

Conrad, W. K., Nicholls, I. A., and Wall, V. J.: Water-saturated and -undersaturated melting of metaluminous and peraluminous crustal compositions at 10 kb: evidence for the origin of silisic magmas in the Taupo Volcanic Zone, New Zealand, and other occurrences, J. Petrol., 29, 765–803, https://doi.org/10.1093/petrology/29.4.765, 1988.

Defant, M. J. and Drummond, M. S.: Derivation of some modern arc magmas by melting of young subducted lithosphere, Nature, 347, 662–665, https://doi.org/10.1038/347662a0, 1990.

Douce, A. E. P.: Generation of metaluminous A-type granites by low-pressure melting of calc-alkaline granitoids, Geology, 25, 743–746, https://doi.org/10.1130/0091-7613(1997)025<0743:GOMATG>2.3.CO;2, 1997.

Drummond, M. S., Defant, M. J., and Kepezhinskas, P. K.: Petrogenesis of slab-derived trondhjemite–tonalite–dacite/adakite magmas, T. Roy. Soc. Edin., 87, 205–215, https://doi.org/10.1017/S0263593300006611, 1996.

Faure, M., Lin, W., Moni, P., and Bruguier, O.: Paleoproterozoic arc magmatism and collision in Liaodong Peninsula, NE China, Terra Nova, 16, 75–80, https://doi.org/10.1111/j.1365-3121.2004.00533.x, 2004.

Ferry, J. M. and Watson, E. B.: New thermodynamic models and revised calibrations for the Ti-in-zircon and Zr-in-rutile thermometers, Contrib. Mineral. Petr., 154, 429–437, https://doi.org/10.1007/s00410-007-0201-0, 2007.

Gao, S., Rudnick, R. L., Yuan, H. L., Liu, X. M., Liu, Y. S., Xu, W. L., Ling, W. L., Ayers, J. C., Wang, X. C., and Wang, Q. H.: Recycling lower continental crust in the North China craton, Nature, 432, 892–897, https://doi.org/10.1038/nature03162, 2004.

Gao, Y. F., Hou, Z. Q., Kamber, B. S., Wei, R. H., Meng, X.J., and Zhao, R. S.: Adakite-like porphyries from the southern Tibetan continental collision zones: evidence for slab melt metasomatism, Contrib. Mineral. Petr., 153, 105–120, https://doi.org/10.1007/s00410-006-0137-9, 2007.

Griffin, W. L., Belousova, E. A., Shee, S. R., Pearson, N. J., and O'Reilly, S. Y.: Archean crustal evolution in the northern Yilgarn Craton: U-Pb and Hf-isotope evidence from detrital zircons, Precambrian. Res., 131, 231–282, https://doi.org/10.1016/J.PRECAMRES.2003.12.011, 2004.

He, P. L., Huang, X. L., Yang, F., and Wang, X.: Mineralogy constraints on magmatic processes controlling adakitic features of Early Permian high-magnesium diorites in the Western Tianshan orogenic belt, J. Petrol., 61, a114, https://doi.org/10.1093/petrology/egaa114, 2021.

Hoskin, P. W. and Schaltegger, U.: The composition of zircon and igneous and metamorphic petrogenesis, Rev. Mineral. Geochem., 53, 27–62, https://doi.org/10.2113/0530027, 2003.

Hoskin, P. W. O.: Trace-element composition of hydrothermal zircon and the alteration of Hadean zircon from the Jack Hills, Australia, Geochim. Cosmochim. Ac., 69, 637–648, https://doi.org/10.1016/j.gca.2004.07.006, 2005.

Huang, F. and He, Y. S.: Partial melting of the dry mafic continental crust: Implications for petrogenesis of C-type adakites, Chinese Sci. Bull., 55, 1255–1267, https://doi.org/10.1007/s11434-010-3224-2, 2010.

Jackson, S. E., Pearson, N. J., Griffin W L, and Belousova, E. A.: The application of laser ablation-inductively coupled plasma-mass spectrometry to in situ U-Pb zircon geochronology, Chem. Geol., 211, 47–69, https://doi.org/10.1016/j.chemgeo.2004.06.017, 2004.

Jiang, H., Jiang, S. Y., Li, W. Q., Zhao, K. D., and Peng, N. J.: Highly fractionated Jurassic I-type granites and related tungsten mineralization in the Shirenzhang deposit, northern Guangdong, South China: Evidence from cassiterite and zircon U-Pb ages, geochemistry and Sr-Nd-Pb-Hf isotopes, Lithos, 312–313, 186–203, https://doi.org/10.1016/j.lithos.2018.04.030, 2018.

Jiang, Y. H., Jiang, S. Y., Zhao, K. D., Ni, P., Ling, H. F., and Liu, D. Y.: SHRIMP U-Pb zircon dating for lamprophyre from Liaodong Peninsula: Constraints on the initial time of Mesozoic lithosphere thinning beneath eastern China, Chinese Sci. Bull., 50, 2612–2620, https://doi.org/10.1360/982005-373, 2005.

Kamei, A., Miyake, Y., Owada, M., and Kimura, J.: A pseudo adakite derived from partial melting of tonalitic to granodioritic crust, Kyushu, southwest Japan arc, Lithos, 112, 615–625, https://doi.org/10.1016/j.lithos.2009.05.024, 2009.

Kay, R. W. and Kay, S. M.: Delamination and delamination magmatism, Tectonophysics, 219, 177–189, https://doi.org/10.1016/0040-1951(93)90295-U, 1993.

King, S. D., Frost, D. J., and Rubie D. C.: Why cold slabs stagnate in the transition zone, Geology, 43, 231–234, https://doi.org/10.1130/G36320.1, 2015.

Li, C. M., Zhang, C. H., Cope, T. D., and Lin, Y.: Out-of-sequence thrusting in polycyclic thrust belts: An example from the Mesozoic Yanshan belt, North China Craton, Tectonics, 35, 2082–2116, https://doi.org/10.1002/2016TC004187, 2016.

Li, S. Z. and Zhao, G. C.: SHRIMP U-Pb zircon geochronology of the Liaoji granitoids: Constraints on the evolution of the Paleoproterozoic Jiao-Liao-Ji belt in the Eastern Block of the North China Craton, Precambrian. Res., 158, 1–16, https://doi.org/10.1016/j.precamres.2007.04.001, 2007.

Li, S. Z., Liu, J. Z., Zhao, G. C., Wu, F. Y., Han, Z. Z., and Yang, Z. Z.: Key geochronology of Mesozoic deformation in the eastern block of the North China Craton and its constraints on regional tectonics: A case of Jiaodong and Liaodong Peninsula, Acta. Petrol. Sin., 2, 633–646, https://doi.org/10.1007/BF02873097, 2004.

Li, S. Z., Zhao, G. C., Sun, M., Han, Z. Z., Hao, D. F., Luo, Y., and Xia, X. P.: Deformation history of the Paleoproterozoic Liaohe Group in the Eastern Block of the North China Craton, J. Asian Earth. Sci., 24, 659–674, https://doi.org/10.1016/j.jseaes.2003.11.008, 2005.

Li, X. H., Long, W. G., Li, Q. L., Liu, Y., Zheng, Y. F., Yang, Y. H., Chamberlain, K. R., Wan, D. F., Guo, C. H., and Wang, X. C.: Penglai Zircon Megacrysts: A Potential New Working Reference Material for Microbeam Determination of Hf-O Isotopes and U-Pb Age, Geostand. Geoanal. Res., 34, 117–134, https://doi.org/10.1111/j.1751-908X.2010.00036.x, 2010.

Li, Z., Chen, B., Liu, J. W., Zhang, L., and Yang, C.: Zircon U-Pb ages and their implications for the South Liaohe Group in the Liaodong Peninsula, Northeast China, Acta Petrol. Sin., 31, 1589–1605, 2015 (in Chinese with English abstract).

Liu, Y. S., Hu, Z. C., Zong, K. Q., Gao, C. G., Gao, S., Xu, J., and Chen, H. H.: Reappraisement and refinement of zircon U-Pb isotope and trace element analyses by LA-ICP-MS, Chinese Sci. Bull., 55, 1535–1546, https://doi.org/10.1007/s11434-010-3052-4, 2010.

Loader, M. A., Wilkinson, J. J., and Armstrong, R. N.: The effect of titanite crystallisation on Eu and Ce anomalies in zircon and its implications for the assessment of porphyry Cu deposit fertility, Earth. Planet. Sc. Lett., 472, 107–119, https://doi.org/10.1016/j.epsl.2017.05.010, 2017.

Ludwig, K. R.: User's manual for Isoplot 3.00: a geochronological toolkit for Microsoft Excel, Spec. Publ./Berkeley Geochronol. Cent., 4, Kenneth R. Ludwig, Berkeley, Calif, 2003.

Ma, L., Jiang, S. Y., Dai, B. Z., Jiang, Y. H., Hou, M. L., Pu, W., and Xu, B.: Multiple sources for the origin of Late Jurassic Linglong adakitic granite in the Shandong Penin-

sula, eastern China: Zircon U-Pb geochronological, geochemical and Sr-Nd-Hf isotopic evidence, Lithos, 162–163, 251–263, https://doi.org/10.1016/j.lithos.2013.01.009, 2013.

Ma, Q., Zheng, J. P., Griffin, W. L., Zhang, M., Tang, H. Y., Su, Y. P., and Ping, X. Q.: Triassic "adakitic" rocks in an extensional setting (North China): Melts from the cratonic lower crust, Lithos, 149, 159–173, https://doi.org/10.1016/j.lithos.2012.04.017, 2012.

Ma, Q., Zheng, J. P., Xu, Y. G., Griffin, W. L., and Zhang, R. S.: Are continental "adakites" derived from thickened or foundered lower crust?, Earth. Planet. Sc. Lett., 419, 125–133, https://doi.org/10.1016/j.epsl.2015.02.036, 2015.

Ma, X. H., Chen, B., and Yang, M. C.: Magma mixing origin for the Aolunhua porphyry related to Mo-Cu mineralization, eastern Central Asian Orogenic Belt, Gondwana. Res., 24, 1152–1171, https://doi.org/10.1016/j.gr.2013.02.010, 2013.

Macpherson, C. G., Dreher, S. T., and Thirlwall, M. F.: Adakites without slab melting: High pressure differentiation of island arc magma, Mindanao, the Philippines, Earth. Planet. Sc. Lett., 243, 581–593, https://doi.org/10.1016/j.epsl.2005.12.034, 2006.

Mahon, K. I.: The New "York" regression: Application of an improved statistical method to geochemistry, Int. Geol. Rev., 38, 293–303, https://doi.org/10.1080/00206819709465336, 1996.

Maniar, P. D. and Piccoli, P. M.: Tectonic discrimination of granitoids, Geol. Soc. Am. Bull., 101, 635–643, https://doi.org/10.1130/0016-7606(1989)101<0635:TDOG>2.3.CO;2, 1989.

Martin, H., Smithies, R. H., Rapp, R., Moyen, J.-F., and Champion, D.: An overview of adakite, tonalite-trondhjemite-granodiorite (TTG), and sanukitoid: relationships and some implications for crustal evolution, Lithos, 79, 1–24, https://doi.org/10.1016/j.lithos.2004.04.048, 2005.

Meng, E., Liu, F. L., Liu, P. H., Liu, C. H., Yang, H., Wang, F., Shi, J. R., and Cai, J.: Petrogenesis and tectonic significance of Paleoproterozoic meta-mafic rocks from central Liaodong Peninsula, northeast China: Evidence from zircon U-Pb dating and in situ Lu-Hf isotopes, and whole-rock geochemistry, Precambrian. Res., 247, 92–109, https://doi.org/10.1016/j.precamres.2014.03.017, 2014.

Meng, Q. R.: What drove late Mesozoic extension of the northern China-Mongolia tract?, Tectonophysics, 369, 155–174, https://doi.org/10.1016/S0040-1951(03)00195-1, 2003.

Mezger, K. and Krogstad, E. J.: Interpretation of discordant U-Pb zircon ages: An evaluation, J. Metamorph. Geol., 15, 127–140, https://doi.org/10.1111/j.1525-1314.1997.00008.x, 1997.

Middlemost, E. A. K.: Naming materials in the magma/igneous rock system, Earth-Sci. Rev., 37, 215–224, https://doi.org/10.1016/0012-8252(94)90029-9, 1994.

Miller, C. F., McDowell, S. M., and Mapes, R. W.: Hot and cold granites? Implications of zircon saturation temperatures and preservation of inheritance, Geology, 31, 529–532, https://doi.org/10.1130/0091-7613(2003)031<0529:hacgio>2.0.co;2, 2003.

Miller, J. F. and Harris, N. B. W.: Evolution of continental crust in the Central Andes; constraints from Nd isotope systematics, Geology, 17, 615–617, https://doi.org/10.1130/0091-7613(1989)017<0615:EOCCIT>2.3.CO;2, 1989.

Moyen, J.: High Sr/Y and La/Yb ratios: The meaning of the "adakitic signature", Lithos, 112, 556–574, https://doi.org/10.1016/j.lithos.2009.04.001, 2009.

Nakamura, H. and Iwamori, H.: Generation of adakites in a cold subduction zone due to double subducting plates, Contrib. Mineral. Petr., 165, 1107–1134, https://doi.org/10.1007/s00410-013-0850-0, 2013.

Nasdala, L., Pidgeon, R. T., Wolf, D., and Irmer, G., Metamictization and U-Pb isotopic discordance in single zircons: a combined Raman microprobe and SHRIMP ion probe study, Miner. Petrol., 62, 1–27, https://doi.org/10.1007/BF01173760, 1998.

Nash, D. J., Ciborowski, T., Ullyott, J. S., Pearson, M. P., and Whitaker, K. A.: Origins of the sarsen megaliths at Stonehenge, Sci. Adv., 6, eabc0133, https://doi.org/10.1126/sciadv.abc0133, 2020.

Ou, Q., Wang, Q., Wyman, D. A., Zhang, H. X., Yang, J. H., Zeng, J. P., Hao, L. L., Chen, Y. W., Liang, H., and Qi, Y.: Eocene adakitic porphyries in the central-northern Qiangtang Block, central Tibet: Partial melting of thickened lower crust and implications for initial surface uplifting of the plateau, J. Geophys. Res.-Sol. Ea., 122, 1025–1053, https://doi.org/10.1002/2016JB013259, 2017.

Parsons, B. and McKenzie, D.: Mantle convection and the thermal structure of the plates, J. Geophys. Res.-Sol. Ea., 83, 4485–4496, https://doi.org/10.1029/JB083iB09p04485, 1978.

Patiño Douce, A. E. P.: What do experiments tell us about the relative contributions of crust and mantle to the origin of granitic magmas?, Geol. Soc. Lond. Spec. Publ., 168, 55–75, https://doi.org/10.1144/GSL.SP.1999.168.01.05, 1999.

Qiu, L., Kong, R. Y., Yan, D. P., Wells, M. L., Wang, A. P., Sun, W. H., Yang, W. X., Han, Y. G., Li, C. M., and Zhang, Y. X.: The Zhayao tectonic window of the Jurassic Yuantai thrust system in Liaodong Peninsula, NE China: Geometry, kinematics and tectonic implications, J. Asian Earth Sci., 164, 58–71, https://doi.org/10.1016/j.jseaes.2018.06.012, 2018.

Rapp, R. P., Shimizu, N., and Norman, M. D.: Growth of early continental crust by partial melting of eclogite, Nature, 425, 605–609, https://doi.org/10.1038/nature02031, 2003.

Ren, Z. H., Lin, W., Faure, M., Meng, L. T., Qiu, H. B., and Zeng, J. P.: Triassic-Jurassic evolution of the eastern North China Craton: Insights from the Lushun-Dalian area, South Liaodong Peninsula, NE China, Geol. Soc. Am. Bull., 133, 393–408, https://doi.org/10.1130/B35533.1, 2020.

Rudnick, R. L. and Gao, S.: Composition of the continental crust, Treatise. Geochem., 3, 1–64, https://doi.org/10.1016/b0-08-043751-6/03016-4, 2003.

Schiller, D. and Finger, F.: Application of Ti-in-zircon thermometry to granite studies: problems and possible solutions, Contrib. Mineral. Petr., 174, 51, https://doi.org/10.1007/s00410-019-1585-3, 2019.

Schmitz, M. D. and Kuiper, K. F.: High-Precision Geochronology, Elements, 9, 25–30, https://doi.org/10.2113/gselements.9.1.25, 2013.

Schwartz, J. J., Johnson, K., Miranda, E. A., and Wooden, J. L.: The generation of high Sr/Y plutons following Late Jurassic arc–arc collision, Blue Mountains province, NE Oregon, Lithos, 126, 22–41, https://doi.org/10.1016/j.lithos.2011.05.005, 2011.

Scott, E. M., Allen, M. B., Macpherson, C. G., McCaffrey, K. J. W., Davidson, J. P., Saville, C., and Ducea, M. N.: Andean surface uplift constrained by radiogenic isotopes of arc lavas, Nat.

Commun., 9, 969, https://doi.org/10.1038/s41467-018-03173-4, 2018.

Shahbazi, H., Maghami, Y. T., Azizi, H., Asahara, Y., Siebel, Y., Maanijou, M., and Rezai, A.: Zircon U-Pb ages and petrogenesis of late Miocene adakitic rocks from the Sari Gunay gold deposit, NW Iran, Geol. Mag., 158, 1733–1755, https://doi.org/10.1017/S0016756821000297, 2021.

Shannon, R. D.: Revised effective ionic radii and systematic studies of interatomic distances in halides and chalcogenides, Acta Crystallogr. A, 32, 751–767, https://doi.org/10.1107/S0567739476001551, 1976.

Shaw, D. M.: Trace element fractionation during anatexis, Geochim. Cosmochim. Ac., 34, 237–243, https://doi.org/10.1016/0016-7037(70)90009-8, 1970.

Siégel, C., Bryan, S. E., Allen, C. M., and Gust, D. A.: Use and abuse of zircon-based thermometers: A critical review and a recommended approach to identify antecrystic zircons, Earth. Sci. Rev., 176, 87–116, https://doi.org/10.1016/j.earscirev.2017.08.011, 2018.

Skjerlie, K. P. and Johnston, A. D.: Vapor-absent melting at 10 kbar of a biotite-and amphibole-bearing tonalitic gneiss: implications for the generation of A-type granites, Geology, 20, 263–266, https://doi.org/10.1130/0091-7613(1992)020<0263:VAMAKO>2.3.CO;2, 1992.

Sláma, J., Košler, J., and Condon, D. J.: Plešovice zircon-A new natural reference material for U-Pb and Hf isotopic microanalysis, Chem. Geol., 249, 1–35, https://doi.org/10.1016/j.chemgeo.2007.11.005, 2008.

Söderlund, U., Patchett, P. J., Vervoort, J. D., and Isachsen, C. E.: The 176 Lu decay constant determined by Lu-Hf and U-Pb isotope systematics of Precambrian mafic intrusions, Earth. Planet. Sc. Lett., 219, 311–324, https://doi.org/10.1016/S0012-821X(04)00012-3, 2004.

Sun, S. S. and McDonough, W. F.: Chemical and isotopic systematics of oceanic basalts: implications for mantle composition and processes, Geol. Soc. Lond. Spec. Publ., 42, 313–345, https://doi.org/10.1144/GSL.SP.1989.042.01.19, 1989.

Tang, J., Xu, W. L., Wang, F., and Ge, W. C.: Subduction history of the Paleo-Pacific slab beneath Eurasian continent: Mesozoic-Paleogene magmatic records in Northeast Asia, Sci. China. Earth. Sci., 61, 527–559, https://doi.org/10.1007/s11430-017-9174-1, 2018.

Trail, D., Watson, E. B., and Tailby, N. D.: Ce and Eu anomalies in zircon as proxies for the oxidation state of magmas, Geochim. Cosmochim. Ac., 97, 70–87, https://doi.org/10.1016/j.gca.2012.08.032, 2012.

Vervoort, J. D. and Blichert-Toft, J.: Evolution of the depleted mantle: Hf isotope evidence from juvenile rocks through time, Geochim. Cosmochim. Ac., 63, 533–556, https://doi.org/10.1016/S0016-7037(98)00274-9, 1999.

Wan, Y. S., Song, B., Liu, D. Y., Wilde, S. A., Wu, J. S., Shi, Y. R., Yin, X. Y., and Zhou, H. Y.: SHRIMP U-Pb zircon geochronology of Palaeoproterozoic metasedimentary rocks in the North China Craton: Evidence for a major Late Palaeoproterozoic tectonothermal event, Precambrian. Res., 149, 271, https://doi.org/10.1016/j.precamres.2006.06.006, 2006.

Wang, F., Liu, F., Schertl, H. P., Xu, W., Liu, P., and Tian, Z.: Detrital zircon U-Pb geochronology and Hf isotopes of the Liaohe Group, Jiao-Liao-Ji Belt: Implications for the Paleoproterozoic tectonic evolution, Precambrian. Res., 340, 105633, https://doi.org/10.1016/j.precamres.2020.105633, 2020.

Wang, N., Wu, C. L., Lei, M., and Chen, H. J.: Petrogenesis and tectonic implications of the Early Paleozoic granites in the western segment of the North Qilian orogenic belt, China, Lithos, 312–313, 89–107, https://doi.org/10.1016/j.lithos.2018.04.023, 2018.

Wang, Q., Xu, J. F., Jian, P., Bao Z. W., Zhao, Z. H., Li, C. F., Xiong, X. L., and Ma, J. L.: Petrogenesis of adakitic porphyries in an extensional tectonic setting, Dexing, South China: Implications for the genesis of porphyry copper mineralization, J. Petrol., 47, 119–144, https://doi.org/10.1093/petrology/egi070, 2006.

Wang, X., Griffin, W. L., O'Reilly, S. Y., and Li, W. X.: Three stages of zircon growth in magmatic rocks from the Pingtan Complex, eastern China, Acta Geol. Sin.-Engl., 81, 68–80, https://doi.org/10.3321/j.issn:1000-9515.2007.01.008, 2007.

Wang, X., Griffin, W. L., Chen, J., Huang, P. Y., and Li, X.: U and Th contents and Th/U ratios of zircon in felsic and mafic magmatic rocks: Improved zircon-melt distribution coefficients, Acta Geol. Sin.-Engl., 85, 164–174, https://doi.org/10.1111/j.1755-6724.2011.00387.x, 2011.

Wang, X. L., Lv, X., Liu, Y. J., Zhao, Y. Y., Li, C., Wu, W. B., Wang, Y. P., and Li, H. Y.: LA-ICP-MS zircon U-Pb ages, geochemical characteristics of Late Triassic intrusives in Xiuyan area, eastern Liaoning and their geological significances, Ore. Geol. Rev., 65, 401–416, https://doi.org/10.16509/j.georeview.2019.02.010, 2019.

Wang, X. P., Oh, C. W., Peng, P., Zhai, M. G., Wang, X. H., and Lee, B. Y.: Distribution pattern of age and geochemistry of 2.18–2.14 Ga I- and A-type granites and their implication for the tectonics of the Liao-Ji belt in the North China Craton, Lithos, 364–365, 105518, https://doi.org/10.1016/j.lithos.2020.105518, 2020.

Watson, E. B. and Harrison, T. M.: Zircon saturation revisited: temperature and composition effects in a variety of crustal magma types, Earth. Planet. Sc. Lett., 64, 295–304, https://doi.org/10.1016/0012-821X(83)90211-X, 1983.

Watson, E. B. and Harrison, T. M.: Zircon thermometer reveals minimum melting conditions on earliest Earth, Science, 308, 841–844, https://doi.org/10.1126/science.1110873, 2005.

Whalen, J. B., Currie, K. L., and Chappell, B. W.: A-type granites: geochemical characteristics, discrimination and petrogenesis, Contrib. Mineral. Petr., 95, 407–419, https://doi.org/10.1007/BF00402202, 1987.

Wolf, M. B. and London, D.: Apatite dissolution into peraluminous haplogranitic melts: An experimental study of solubilities and mechanisms, Geochim. Cosmochim. Ac., 58, 4127–4145, https://doi.org/10.1016/0016-7037(94)90269-0, 1994.

Wu, F. Y., Jahn, B. M., Wilde, S. A., Lo, C. H., Yui, T. F., Lin, Q., Ge, W. C., and Sun, D. Y: Highly fractionated I-type granites in NE China (I): geochronology and petrogenesis, Lithos, 66, 241–273, https://doi.org/10.1016/s0024-4937(02)00222-0, 2003.

Wu, F. Y., Yang, J. H., Wilde, S. A., and Zhang, X. O.: Geochronology, petrogenesis and tectonic implications of Jurassic granites in the Liaodong Peninsula, NE China, Chem. Geol., 221, 127–156, https://doi.org/10.1016/j.chemgeo.2005.04.010, 2005a.

Wu, F. Y., Yang, J. H., and Liu, X. M.: Geochronological framework of the Mesozoic granitic magmatism in the Liaodong Peninsula, Northeast China, Geol. J. China. Univ., 11, 305–317, 2005b (in Chinese with English abstract).

Wu, F. Y., Lin, J. Q., Wilde, S. A., Zhang, X. O., and Yang, J. H.: Nature and significance of the Early Cretaceous giant igneous event in eastern China, Earth. Planet. Sc. Lett., 233, 103–119, https://doi.org/10.1016/j.epsl.2005.02.019, 2005c.

Wu, F. Y., Yang, Y. H., Xie, L. W., Yang, J. H., and Xu, P.: Hf isotopic compositions of the standard zircons and baddeleyites used in U-Pb geochronology, Chem. Geol., 234, 105–126, https://doi.org/10.1016/j.chemgeo.2006.05.003, 2006.

Wu, F. Y., Han, R. H., Yang, J. H., Wilde, S. A., Zhai, M. G., and Park, S. C.: Initial constraints on the timing of granitic magmatism in North Korea using U-Pb zircon geochronology, Chem. Geol., 238, 232–248, https://doi.org/10.1016/j.chemgeo.2006.11.012, 2007.

Wu, F. Y., Liu, X. C., Ji, W. Q., Wang, J. M., and Yang, L.: Highly fractionated granites: Recognition and research, Sci. China. Earth. Sci., 60, 1201–1219, https://doi.org/10.1007/s11430-016-5139-1, 2017.

Xu, J. F., Shinjo, R., Defant, M. J., Wang, Q., and Rapp, R. P.: Origin of Mesozoic adakitic intrusive rocks in the Ningzhen area of east China: partial melting of delaminated lower continental crust?, Geology, 30, 1111–1114, https://doi.org/10.1130/0091-7613(2002)030<1111:OOMAIR>2.0.CO;2, 2002.

Xue, S., Ling, M. X., Liu, Y. L., Zhang, H., and Sun, W. D.: The genesis of early Carboniferous adakitic rocks at the southern margin of the Alxa Block, North China, Lithos, 278–281, 181–194, https://doi.org/10.1016/j.lithos.2017.01.012, 2017.

Xue, J. X., Liu, Z. H., Liu, J. X., Dong, X. J., Feng, F., and Lian, G. H.: Geochemistry, Geochronology, Hf isotope and Tectonic Significance of the Late Jurassic Huangdi Pluton in Xiuyan, Liaodong Penins, Earth Sci., 46, 2030–2043, https://doi.org/10.3799/dqkx.2020.008, 2020 (in Chinese with English abstract).

Yang, F. C., Song, Y. H., Hao, L. B., and Peng, C.: Late Jurassic SHRIMP U-Pb age and Hf isotopic characteristics of granite from the Sanjiazi Area in Liaodong and their geological significance, Acta. Geol. Sin.-Eng., 89, 1773–1782, 2015 (in Chinese with English abstract).

Yang, F. C., Song, Y. H., Yang, J. L., Shen, X., and Gu, Y. C.: SHRIMP U-Pb age and geochemical characteristics of granites in Wulong-Sidaogou Gold Deposit, East Liaoning, Geotectonica et Metallogenia, 42, 940–954, https://doi.org/10.16539/j.ddgzyckx.2018.05.010, 2018 (in Chinese with English abstract).

Yang, J. H., Wu, F. Y., Lo, C. H., Chung, S. L., Zhang, Y. B., and Wilde, S. A.: Deformation age of Jurassic granites in the Dandong area, eastern China: Ar−40/Ar−39 geochronological constraints, Acta Petrol. Sin., 20, 1205–1214, 2004 (in Chinese with English abstract).

Yang, J. H., Wu, F. Y., Xie, L. W., and Liu, X. M.: Petrogenesis and tectonic implications of Kuangdonggou synites in the Liaodong Peninsula, east North China Craton: Constraints from in-suit zircon U-Pb ages and Hf isotopes, Acta Petrol. Sin., 23, 263–276, https://doi.org/10.1016/j.sedgeo.2006.03.028, 2007 (in Chinese with English abstract).

Yang, M. C., Chen, B., and Yan, C.: Petrological, geochronological, geochemical and Sr-Nd-Hf isotopic constraints on the petrogenesis of the Shuangcha Paleoproterozoic megaporphyritic granite in the southern Jilin Province: Tectonic implications, Acta Petrol. Sin., 31, 1573–1588, 2015 (in Chinese with English abstract).

Yang, M. C., Chen, B., and Yan, C.: Paleoproterozoic Gneissic Granites in the Liaoji Mobile Belt, North China Craton: Implications for Tectonic Setting, in: Main Tectonic Events and Metallogeny of the North China Craton, edited by: Zhai, M., Zhao, Y., and Zhao, T., Geology, Springer, Singapore, 155–180, https://doi.org/10.1007/978-981-10-1064-4_7, 2016.

Yang, Y. W., Yu, C., Wang, G. W., Su, T., Yang, X. Y., and Zhang, T. Y.: Chronology, geochemistry and zircon Hf isotopes of the Paleoproterozoic alkali feldspar granite from the Heigou area in the eastern Liaoning Province:constraints on the tectonic evolution of the Liao-Ji orogenic belt, Acta. Geol. Sin., https://doi.org/10.19762/j.cnki.dizhixuebao.2020020, 2020 (in Chinese with English abstract).

Yu, S., Zhang, J., and Del Real, P. G.: Geochemistry and zircon U-Pb ages of adakitic rocks from the Dulan area of the North Qaidam UHP terrane, north Tibet: constraints on the timing and nature of regional tectonothermal events associated with collisional orogeny, Gondwana Res., 21, 167–179, https://doi.org/10.1016/j.gr.2011.07.024, 2012.

Yuan, H. L., Gao, S., Dai, M. N., Zong, C. L., Günther, D., Fontaine, G. H., Liu, X. M., and Diwu, C. R.: Simultaneous determinations of U-Pb age, Hf isotopes and trace element compositions of zircon by excimer laser-ablation quadrupole and multiple-collector ICP-MS, Chem. Geol., 247, 100–118, https://doi.org/10.1016/j.chemgeo.2007.10.003, 2008.

Yuan, L. L., Zhang, X. H., Xue, F. H., Han, C. M., Chen, H. H., and Zhai, M. G.: Two episodes of Paleoproterozoic mafic intrusions from Liaoning province, North China Craton: Petrogenesis and tectonic implications, Precambrian Res., 264, 119–139, https://doi.org/10.1016/j.precamres.2015.04.017, 2015.

Zeng, R. Y., Lai, J. Q., Mao, X. C., Li, B., Ju, P. J., and Tao, S. L.: Geochemistry, zircon U-Pb dating and Hf isotopies composition of Paleozoic granitoids in Jinchuan, NW China: Constraints on their petrogenesis, source characteristics and tectonic implication, J. Asian Earth. Sci., 121, 20–33, https://doi.org/10.1016/j.jseaes.2016.02.009, 2016.

Zeng, R. Y., Lai, J. Q., Mao, X. C., Li, B., Zhang, J. D., Bayless, R., and Yang, L. Z.: Paleoproterozoic Multiple Tectonothermal Events in the Longshoushan Area, Western North China Craton and Their Geological Implication: Evidence from Geochemistry, Zircon U-Pb Geochronology and Hf Isotopes, Minerals Basel, 8, 361, https://doi.org/10.3390/MIN8090361, 2018.

Zhai, M. G., Meng, Q. R., Liu, J. M., Hou, Q. L., Hu, S. B., Li, Z., Zhang, H. F., Liu, W., Shao, J. A., and Zhu, R. X.: Geological features of Mesozoic tectonic regime inversion in eastern North China and implication for geodynamics, Earth Sci. Front., 11, 285–298, https://doi.org/10.3321/j.issn:1005-2321.2004.03.027, 2004.

Zhan, Q. Y., Zhu, D. C., Wang, Q., Weinberg, R. F., Xie, J. C., Li, S. M., Zhang, L. L., and Zhao, Z. D.: Source and pressure effects in the genesis of the Late Triassic high Sr/Y granites from the Songpan-Ganzi Fold Belt, eastern Tibetan Plateau, Lithos, 368–369, https://doi.org/10.1016/j.lithos.2020.105584, 2020.

Zhang, B., Guo, F., Zhang, X. B., Wu, Y. M., Wang, G. Q., and Zhao, L.: Early Cretaceous subduction of Paleo-Pacific Ocean in the coastal region of SE China: Petrological and geochemical constraints from the mafic intrusions, Lithos, 334–335, 8–24, https://doi.org/10.1016/j.lithos.2019.03.010, 2019.

Zhang, Q., Qian, Q., Wang, E. Q., Wang, Y., Zhao, T. P., Hao, J., and Guo, G. J.: An East China plateau in mid-late Yanshanian period: implication from adakites, Chinese, Chinese Journal of Geology, 36, 248–255, 2001 (in Chinese with English abstract).

Zhang, Q., Wang, Y., Liu, H., and Wang, Y.: On the space-time distribution and geodynamic environments of adakites in China annex: controversies over differing opinions for adakites in China, Earth Sci. Front., https://doi.org/10.1016/S0955-2219(02)00073-0, 2003 (in Chinese with English abstract).

Zhang, S., Zhu, G., Xiao, S. Y., Su, N., Liu, C., Wu, X. D., Yin, H., Li, Y. J., and Lu, Y. C.: Temporal variations in the dynamic evolution of an overriding plate: Evidence from the Wulong area in the eastern North China Craton, China, Geol. Soc. Am. Bull., 132, 2023–2042, https://doi.org/10.1130/B35465.1, 2020.

Zhao, K. D., Jiang, S. Y., Ling, H. F., and Palmer, M. R.: Reliability of LA-ICP-MS U-Pb dating of zircons with high U concentrations: A case study from the U-bearing Douzhashan Granite in South China, Chem. Geol., 389, 110–121, https://doi.org/10.1016/j.chemgeo.2014.09.018, 2014.

Zheng, J. P. and Dai, H. K.: Subduction and retreating of the western Pacific plate resulted in lithospheric mantle replacement and coupled basinmountain respond in the North China Craton, Sci. China. Earth. Sci., 61, 406–424, https://doi.org/10.1007/s11430-017-9166-8, 2018.

Zheng, Y. F., Xu, Z. F., Zhao, Z. F., and Dai, L. Q.: Mesozoic mafic magmatism in North China: Implications for thinning and destruction of cratonic lithosphere, Sci. China. Earth Sci., 61, 353–385, https://doi.org/10.1007/s11430-017-9160-3, 2018.

Zhu, R. X. and Xu, Y. G.: The subduction of the west Pacific plate and the destruction of the North China Craton, Sci. China. Earth Sci., 62, 1340–1350, https://doi.org/10.1007/s11430-018-9356-y, 2019.